

Nonparametric Bayes Differential Analysis of Multigroup DNA Methylation Data

Chiyu Gu

Bayer Crop Science, Chesterfield, Missouri

and

Veerabhadran Baladandayuthapani

Department of Biostatistics, University of Michigan

and

Subharup Guha

Department of Biostatistics, University of Florida

May 5, 2023

Abstract

DNA methylation datasets in cancer studies are comprised of measurements on a large number of genomic locations called cytosine-phosphate-guanine (CpG) sites with complex correlation structures. A fundamental goal of these studies is the development of statistical techniques that can identify disease genomic signatures across multiple patient groups defined by different experimental or biological conditions. We propose *BayesDiff*, a nonparametric Bayesian approach for differential analysis relying on a novel class of first order mixture models called the Sticky Pitman-Yor process or two-restaurant two-cuisine franchise (2R2CF). The BayesDiff methodology flexibly utilizes information from all CpG sites or probes, adaptively accommodates any serial dependence due to the widely varying inter-probe distances, and performs simultaneous inferences about the differential genomic signature of the patient groups. Using simulation studies, we demonstrate the effectiveness of the BayesDiff procedure relative to existing statistical techniques for differential DNA methylation. The

methodology is applied to analyze a gastrointestinal (GI) cancer dataset that displays both serial correlations and interaction patterns. The results support and complement known aspects of DNA methylation and gene association in upper GI cancers.

Keywords: 2R2CF; First order models; Mixture models; Sticky Pitman-Yor process; Two-restaurant two-cuisine franchise

1 Introduction

Recent advances in array-based and next-generation sequencing (NGS) technologies have revolutionized biomedical research, especially in cancer. The rapid decline in the cost of genome technologies has facilitated the availability of datasets involving intrinsically different sizes and scales of high-throughput data and provided genome-wide, high resolution information about the biology of cancer. A common analytical goal is the identification of differential genomic signatures between groups of samples corresponding to different treatments or biological conditions, e.g., treatment arms, response to adjuvant chemotherapy, tumor subtypes, or cancer stages. The challenges include the high dimensionality of genomic biomarkers or probes, usually in the hundreds of thousands, and the relatively small number of patient samples, usually no more than a few hundred. This “small n , large p ” setting results in unstable inferences due to collinearity. Further, there exist complex interaction patterns, such as signaling or functional pathway-based interactions, and location-based serial correlation for high-throughput sequencing data. These data attributes significantly affect the reliability of statistical techniques for detecting differential genomic signatures.

Differential DNA methylation in cancer studies DNA methylation is an important epigenetic mechanism that involves the addition of a methyl (CH_3) group to DNA, resulting in the modification of gene functions. It typically occurs at specific genomic locations called cytosine-phosphate-guanine (CpG) sites. Alterations in DNA methylation, e.g., hypomethylation of oncogenes and hypermethylation of tumor suppressor genes, are often associated with the development and progression of cancer (Feinberg & Tycko 2004). It was previously believed that these alterations occur almost exclusively at promoter regions known as CpG islands, i.e., chromosomal regions with high concentrations of CpG sites. However, with the advent of high-throughput technologies, it has been shown that a significant proportion of cancer-related alterations do not occur in promoters or CpG islands (Izarray et al. 2009), prompting higher resolution, epigenome-wide investigations.

Gastrointestinal (GI) cancer, the most common form of cancer in the U.S. (Siegel et al. 2017), refers to malignant conditions affecting the digestive system associated with epigenetic alterations (Vedeld et al. 2017). Molecular characterization of different cancer types, facilitated by the identification of differentially methylated CpG sites, is therefore key to better understanding GI cancer. In the motivating application, we analyze methylation profiles publicly available from The Cancer Genome Atlas (TCGA) project, consisting of 1,224 tumor samples belonging to four GI cancers of the upper digestive tract: stomach adenocarcinoma (STAD), liver hepatocellular carcinoma (LIHC), esophageal carcinoma (ESCA) and pancreatic adenocarcinoma (PAAD). For 485,577 probes, where each probe is mapped to a CpG site, DNA methylation levels or Beta-values ranging from 0 (no methylation) to 1 (full methylation) were measured using the Illumina Human Methylation 450 platform.

Figure 1 displays the methylation levels for CpG sites near TP53, a tumor suppressor gene located on chromosome 17. A random subset of the tumor samples was chosen to facilitate an informal visual evaluation. Each plotted point represents the methylation level of a tumor sample at a CpG site. As indicated in the figure legend, the four sets of colors and shapes of the points represent the four upper GI cancers. The vertical dashed lines indicate the boundaries of the TP53 gene. Although differential methylation is clearly visible at some CpG sites, the differences are generally subtle, demonstrating the need for sophisticated statistical analyses. An obvious feature is the correlation between the apparent

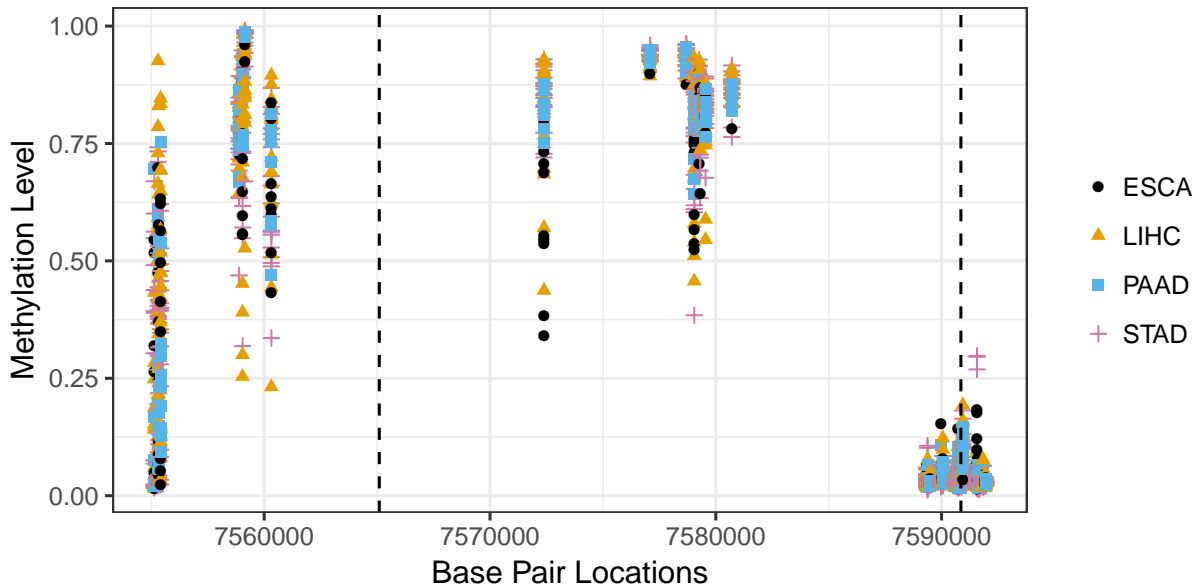


Figure 1: Methylation levels of CpG sites near gene TP53 for randomly chosen tumor samples of the TCGA upper GI dataset. Each plotted point represents the methylation level at a CpG site, with the shapes and colors corresponding to different GI cancers indicated in the legend. The vertical dashed lines demarcate the TP53 gene boundaries.

methylation statuses of nearby CpG sites (Eckhardt et al. 2006, Irizarry et al. 2008, Leek et al. 2010). The dependence of proximal CpG sites is also seen in Figure 6 of Supplementary Material, where we find high first order autocorrelations and highly significant tests for serial correlations. Furthermore, the variability of the inter-probe spacings in Figure 1 suggests that the need to model distance-based dependencies.

Existing statistical approaches for differential DNA methylation and limitations

Numerous frequentist and Bayesian methods have been developed for differential DNA methylation, and can be broadly classified into four categories: (i) *Testing-based methods*, such as Illumina Methylation Analyzer (IMA) (Wang et al. 2012), City of Hope CpG Island Analysis Pipeline (COHCAP) (Warden et al. 2013), and BSmooth (Hansen et al. 2012).

These methods rely on two-sample or multiple-sample tests for the mean group differences at each CpG site. (ii) *Regression based models*, such as MethyKit (Akalin et al. 2012), bump hunting (Jaffe et al. 2012), Biseq (Hebestreit et al. 2013), and RADMeth (Dolzhenko & Smith 2014). After applying smoothing or other adjustments, these methods fit individual regression models for each CpG site and test for significance. (iii) *Beta-binomial model-based methods*, such as MOABS (Sun et al. 2014), DSS (Feng et al. 2014), and methylSig (Park et al. 2014). These methods fit separate models to each CpG site. (iv) *Hidden Markov models (HMMs)*, such as MethPipe (Song et al. 2013), Bisulfighter (Saito et al. 2014), and HMM-DM (Yu & Sun 2016). These methods detect differentially methylated sites based on inferred hidden states.

The aforementioned methods have several deficiencies. By fitting separate models to each probe, most methods ignore the strong correlations between neighboring probes. This reduces the detection power for the relatively small sample sizes. Additionally, beta-binomial, HMM, and most testing-based methods are able to accommodate only two treatments and rely on inefficient adjustments to compare multiple treatments. The methods that account for serial dependence (e.g., HMMs) do not adjust for the widely varying distances between the probes, and instead, assume uniform inter-probe dependencies. The few methods that account for inter-probe distances (e.g., Hansen et al. 2012, Jaffe et al. 2012, Hebestreit et al. 2013) rely on ad hoc parameter-tuning procedures that do not adjust for distinctive data characteristics.

Motivated by these challenges, we propose general and flexible methodology for differential analysis in DNA methylation data, referred to as *BayesDiff*. Rather than fitting a separate model to each CpG site or probe, BayesDiff relies on a global analytical framework for simultaneous inferences on the probes that adapts to the unique data attributes. To diminish collinearity effects and achieve dimension reduction, the probes are allocated to a smaller, unknown number of latent clusters based on the similarities of probes-specific multivariate parameters. Finally, differential state variables of the probes delineate the genomic signature of the disease to fulfil the main inferential goal.

For realistically modeling the probe-cluster allocation mechanism of DNA methylation profiles, we devise an extension of Pitman-Yor processes (PYPs) (Perman et al. 1992) called

the *Sticky PYP* (equivalently, the *two-restaurant two-cuisine franchise*). In addition to accounting for long-range biological interactions, this nonparametric process accommodates distance-based serial dependencies of the probes. Separately for the differential and non-differential probes, it flexibly permits the data to direct the choice between PYPs, and their special case, Dirichlet processes, in finding the best-fitting allocation schemes.

We implement an inferential procedure for Sticky PYPs using a Markov chain Monte Carlo (MCMC) algorithm specifically designed for posterior inferences in the typically large methylation datasets. Simulation results show that our approach significantly outperforms existing methods for multigroup comparisons in data with or without serial correlation. For the motivating TCGA dataset, in addition to confirming known features of DNA methylation and disease-gene associations, the analysis reveals interesting aspects of the biological mechanisms of upper GI cancers.

The rest of the paper is organized as follows. Section 2 describes the BayesDiff approach, with Section 2.1 introducing the Sticky PYP or two-restaurant two-cuisine franchise (2R2CF) for differential DNA methylation. Section 3 outlines an effective inference procedure for detecting differential probes. Section 4 uses artificial datasets with varying noise and correlation levels to assess the accuracy of BayesDiff in detecting disease genomic signatures and makes comparisons with established techniques for DNA methylation data. The motivating upper GI dataset is analyzed using the BayesDiff procedure in Section 5. Finally, conclusions and future related work are discussed in Section 6.

2 The BayesDiff Model

Sequencing technologies measure DNA methylation levels of p biomarkers represented by CpG sites (“probes”) and n matched patient or tissue samples (“individuals”). Usually, p is much larger than n . The methylation levels, which belong to the interval $[0, 1]$, are arranged in an $n \times p$ matrix of proportions, $\mathbf{X} = ((x_{ij}))$, for individuals i and probes j , with the probes sequentially indexed by their genomic locations. The distances between adjacent probes are denoted by e_1, \dots, e_{p-1} , and typically exhibit high variability. For instance, in the upper GI TCGA dataset, the inter-probe distances range from 2 base pairs

to a million base pairs; a base pair is a unit of DNA length consisting of two nucleobases bound to each other by hydrogen bonds (e.g., [Baker et al. 2008](#)).

Each individual i is associated with a known experimental or biological condition (“treatment”) denoted by t_i and taking values in $\{1, \dots, T\}$ with $T \geq 2$. In the motivating TCGA data, there are $T = 4$ upper GI cancer types. We model the logit transformation of the methylation levels, $z_{ij} = \log(x_{ij}/(1 - x_{ij}))$, as follows:

$$z_{ij} \sim N(\xi_i + \chi_j + \theta_{t_i j}, \sigma^2) \quad (1)$$

where ξ_i represents the i th subject’s random effect, χ_j represents the j th probe’s random effect, and $\theta_{t_i j}$ is the random treatment t –probe j interaction effect. The logit-transformed methylation levels differ from M-values ([Du et al. 2010](#)), commonly used in differential analyses, by $1 - \log(2) = 0.306$; however, the key results are identical.

The main inferential goal is the detection of differential probes, i.e., probes j for which the elements of column vector $\boldsymbol{\theta}_j = (\theta_{1j}, \dots, \theta_{Tj})'$ are not all identical. Consequently, we define a binary *differential state variable*, s_j , with $s_j = 1$ indicating that probe j is not differential and $s_j = 2$ indicating that it is differential:

$$s_j = \begin{cases} 1 & \text{if } \theta_{1j} = \theta_{2j} = \dots = \theta_{Tj}, \\ 2 & \text{otherwise,} \end{cases} \quad (2)$$

for $j = 1, \dots, p$. Thus, the key parameters are s_1, \dots, s_p , with the differential genomic signature consisting of the probes for which state $s_j = 2$. Motivated by the distance-dependent correlations of DNA methylation data and deficiencies of existing statistical approaches, this paper fosters a Bayesian nonparametric framework for random effects $\boldsymbol{\theta}_1, \dots, \boldsymbol{\theta}_p$ determining the differential state variables.

Modeling probe clusters

As mentioned, in addition to high-dimensionality, the analytical challenges include pervasive collinearity due to dependencies between physically proximal probes. Additionally,

there are long-range dependencies between non-adjacent probes because of biological interactions, e.g., signaling or functional pathways. To accommodate these dependence structures and extract information from the large number of probes, we allocate the p probes to a much smaller number, q , of latent clusters based on the similarities of the random effects $\boldsymbol{\theta}_j$. We favor clustering to dimension reduction methods such as principal components analysis (PCA). Because each principal component is a linear combination of all p biomarkers, PCA is less useful in cancer research because of its inability to select features, i.e., probes. By contrast, our approach facilitates biological interpretations by identifying CpG sites relevant to the differential genomic signatures between the treatments.

Suppose that an *allocation variable*, c_j , assigns probe j to one of q latent clusters, where q is unknown. The event $[c_j = k]$ signifies that the j^{th} probe belongs to the k^{th} latent cluster, $k = 1, \dots, q$. We assume that the q clusters are associated with *latent vectors*, $\boldsymbol{\lambda}_1, \dots, \boldsymbol{\lambda}_q$, where the probe-specific random effects and cluster-specific latent vectors have the relation:

$$\boldsymbol{\theta}_j = \boldsymbol{\lambda}_k \quad \text{if } c_j = k. \quad (3)$$

That is, all probes within a cluster are assumed to have identical random effects equal to that cluster’s latent vector. The differential state variables of the probes, defined in equation (2), then become a shared attribute of their parent cluster, and clusters as a whole are either differentially or non-differentially methylated. Further, if probe j belongs to cluster k (i.e., $c_j = k$), then the condition $\theta_{1j} = \theta_{2j} = \dots = \theta_{Tj}$ in equation (2) is equivalent to $\lambda_{1k} = \lambda_{2k} = \dots = \lambda_{Tk}$, and differential clusters constitute the set

$$\mathcal{D} = \left\{ k : \lambda_{tk} \neq \lambda_{t'k}, \text{ for some } t \neq t', k = 1, \dots, q \right\}. \quad (4)$$

Mixture models for allocation Bayesian infinite mixture models are a natural choice for allocating p probes to a smaller, unknown number of latent clusters based on their random effects similarities. Dirichlet processes (Ferguson 1973a) are arguably the most frequently used infinite mixture models; see Müller & Mitra (2013, chap. 4) for a comprehensive review. The use of Dirichlet processes to achieve dimension reduction has precedence in the literature, albeit in unrelated applications (see Medvedovic et al. 2004, Kim et al. 2006, Dunson et al. 2008, Dunson & Park 2008, Guha & Baladandayuthapani 2016). Lijoi,

Mena & Prünster (2007a) advocated the use of Gibbs-type priors (Gnedin & Pitman 2006) for accommodating more flexible clustering mechanisms and demonstrated the utility of Pitman-Yor processes (PYPs) in genomic applications. An overview of Gibbs-type priors and characterization of the learning mechanism is provided by De Blasi et al. (2013). Formally, the PYP (Perman et al. 1992) relies on a discount parameter $d \in [0, 1)$, positive mass parameter α , and T -variate base distribution W , and is denoted by $\mathcal{W}(d, \alpha, W)$. The value $d = 0$ yields a Dirichlet process with mass parameter α and base distribution W . Suppose $\theta_1, \dots, \theta_p$ are distributed as $\mathcal{W}(d, \alpha, W)$. The *stick-breaking representation* of $\mathcal{W}(d, \alpha, W)$ is $\theta_j \stackrel{iid}{\sim} \mathcal{P}$, where random distribution \mathcal{P} is the discrete mixture $\sum_{v=1}^{\infty} \pi_v \delta_{\phi_v}$, with δ_{ϕ_v} denoting a point mass located at the atom $\phi_v \stackrel{iid}{\sim} W$. The random stick-breaking probabilities have the form $\pi_1 = V_1$, and $\pi_h = V_h \prod_{v=1}^{h-1} (1 - V_v)$ for $h > 1$, where $V_h \stackrel{indep}{\sim} \text{beta}(1-d, \alpha+hd)$. Guha & Baladandayuthapani (2016) introduced VariScan, a technique that utilizes PYPs and Dirichlet processes for clustering, variable selection, and prediction in high-dimensional regression problems in general, and in gene expression datasets in particular. They also demonstrated that PYPs are overwhelmingly favored to Dirichlet processes in gene expression datasets, which typically exhibit no serial correlation.

Limitations of existing mixture models Although the aforementioned mixture models achieve dimension reduction and account for the long-range biological interactions between non-adjacent probes, a potential drawback is their implicit assumption of a priori exchangeability of the probes. Consequently, these techniques cannot account for the serial correlation in methylation data. Infinite HMMs, such as the hierarchical Dirichlet process hidden Markov model (HDP-HMM) (Teh et al. 2006) and Sticky HDP-HMM (Fox et al. 2011), may be utilized to fill this gap. Although these models are a step in the right direction, they have several undesirable features for differential analysis. *First*, the degree of first order dependence is uniform irrespective of the inter-probe distances. This is unrealistic in methylation datasets where the correlation typically decreases with inter-probe distance (Hansen et al. 2012, Jaffe et al. 2012, Hebestreit et al. 2013). *Second*, an ad hoc exploratory analysis of the GI cancer dataset reveals that the serial correlation in the treatment-probe effects is weaker than the serial dependence between the differential state variables defined

in equation (2). Although there may not be a biological explanation for this phenomenon, this makes sense from a statistical perspective because the differential states are binary functions of the treatment-probe interactions; the differential states are more sensitive in detecting first order dependence even when the higher-dimensional (and noisier) treatment-probe interactions show little or no correlation. This suggests that a hypothetical two-group Markov model, rather than an infinite-group Markov model such as HDP-HMM or Sticky HDP-HMM, would provide a better fit for the data. *Third*, the range of allocation patterns supported by infinite HMMs is relatively limited. In particular, realistic allocation patterns, such as power law decays in the cluster sizes and large numbers of small-sized clusters, a common feature of cancer datasets (Lijoi et al. 2007b), are assigned relatively small prior probabilities by infinite HMMs.

2.1 Sticky PYP: A Two-restaurant, Two-cuisine Franchise (2R2CF) for Differential Analysis

We invent a mixture model called the Sticky PYP. Essentially, this is a cohort of regular PYPs that generates the probe-specific random effects by switching generative PYPs at random locations along the probe sequence. Alternatively, the well-known Chinese restaurant franchise (CRF) metaphor for HDP-HMMs and Sticky HDP-HMMs can be generalized to the *two-restaurant two-cuisine franchise* (2R2CF) to provide an equivalent representation of Sticky PYPs appropriate for differential analysis. We first present a descriptive overview of 2R2CF.

Imagine that a franchise has two restaurants, labeled 1 and 2. Each restaurant consists of two sections, also labeled 1 and 2. Each section serves a single cuisine and its section-cuisine menu consists of infinite dishes. Section 1 at both restaurants exclusively serves cuisine 1. The cuisine 1 menus, along with selection probabilities associated with the dishes, are identical at the two restaurants. Similarly, section 2 at both restaurants exclusively serves cuisine 2, and the cuisine 2 menus are also identical at the restaurants.

A succession of p customers, representing the CpG sites or probes, arrive at the franchise. The waiting times between successive customers represent the inter-probe distances,

e_1, \dots, e_{p-1} . Each customer selects a restaurant and then selects a section (equivalently, cuisine) in the restaurant. Each restaurant section has an infinite number of tables, and a customer may either sit at a table already occupied by previous customers, or sit at a new table. All customers at a table are served the same dish, previously chosen from the section-cuisine menu by the first customer who sat at that table. A customer who sits at a new table is allowed to independently pick a dish from the cuisine menu with a cuisine-specific probability associated with each dish. As a result, multiple tables in a restaurant section may serve the same dish.

Restaurant 1 specializes in cuisine 1. Consequently, section 1 is more popular with restaurant 1 patrons. Similarly, restaurant 2 specializes in cuisine 2, and so, restaurant 2 customers tend to favor section 2 over section 1. By design, if a customer has eaten a cuisine 1 (2) dish, then the next customer is more likely to visit restaurant 1 (2), where cuisine 1 (2) is more popular. In this manner, each customer tends to select the same cuisine as the previous customer.

In the metaphor, cuisine 1 symbolizes the non-differential state and cuisine 2 symbolizes the differential state. The dish that franchise customer j eats represents the probe-specific random effect, θ_j . Since cuisine 1 represents the non-differential state, its dishes are characterized by T -variate random vectors with all equal elements; see equation (2). In contrast, cuisine 2 (differential state) dishes are characterized by T -variate random vectors with at least two unequal elements.

The dependence in the restaurant and cuisine choices of consecutive customers account for long runs of differential or non-differential states in DNA methylation data. However, a customer's influence on the next customer diminishes as the time interval between the two customers increases. That is, the differential statuses of two adjacent probes become statistically independent in the limit as the inter-probe distance grows.

The 2R2CF process is illustrated in Figure 2 and discussed below in greater detail. The following specification conditions on G , an unknown distribution in \mathcal{R} that is assigned a Dirichlet process prior with mass parameter $\beta > 0$ and univariate normal base distribution, $G_0 = N(\mu_G, \tau_G^2)$. The stick-breaking representation of the Dirichlet process implies that

distribution G is almost surely discrete because it has an infinite mixture distribution:

$$G \stackrel{d}{=} \sum_{v=1}^{\infty} \varpi_v \delta_{\zeta_v}, \text{ where } \sum_{v=1}^{\infty} \varpi_v = 1 \text{ and } \zeta_v \stackrel{iid}{\sim} G_0. \quad (5)$$

The distribution of random probabilities, ϖ_v , which depend on mass parameter β , was derived in [Sethuraman \(1994\)](#); see also [Ishwaran & James \(2003\)](#) and [Lijoi & Prünster \(2010\)](#). In the sequel, we condition on distribution G ; equivalently on the probabilities, ϖ_v , and univariate atoms, ζ_v , for $v \in \mathcal{N}$.

Cuisine 1 menu. Recall that cuisine 1 represents the non-differential state, for which the T -variate random vectors (i.e., dishes in the metaphor) has all equal elements. Cuisine 1 menu, with its countably infinite dishes and their associated probabilities, is modeled as follows as a discrete T -variate *menu distribution*, W_1 . With $\mathbf{1}_T$ denoting the column vector of T ones, let

$$\boldsymbol{\vartheta} \mid \psi = \psi \mathbf{1}_T \text{ where } \psi \sim G. \quad (6)$$

Cuisine 1 menu distribution, W_1 , is defined as the law of random vector $\boldsymbol{\vartheta}$. Then $\mathcal{S}_1 = \{\zeta_v \mathbf{1}_T : v \in \mathcal{N}\}$ is the list of available cuisine 1 dishes and the support of W_1 . The selection probability associated with dish $\zeta_v \mathbf{1}_T$ is ϖ_v .

The continuity of base distribution G_0 in equation (5) guarantees that the menu W_1 dishes are unique. The discreteness of distribution G has practical implications for 2R2CF: (a) cuisine 1 consists of discrete dishes, as required, rather than a continuous spectrum, and (b) since section 1 at both the restaurants serve the same menu, the section 1 customers may eat the same dish even if they select different restaurants.

Cuisine 2 menu. As mentioned earlier, cuisine 2 depicts the differential state and its dishes represent T -variate random vectors with at least two unequal elements. Its menu comprises countably infinite cuisine 2 dishes along with their associated probabilities. The menu is therefore modeled by a T -variate distribution, W_2 , satisfying two conditions: (i) it has a countably infinite support, and (ii) each T -variate atom of W_2 has at least two unequal elements. For any given $\boldsymbol{\phi} = (\phi_1, \dots, \phi_T)' \in \mathcal{R}^T$, a probability mass function for

W_2 that satisfies these conditions is

$$W_2(\phi) = \begin{cases} \prod_{t=1}^T G(\phi_t) / (1 - \sum_{v=1}^{\infty} \varpi_v^T) & \text{if } \phi_t \neq \phi_{t'} \text{ for some } t \neq t', \\ 0 & \text{otherwise,} \end{cases} \quad (7)$$

where $G(\phi)$ denotes the mass function of distribution G , represented in equation (5), evaluated at $\phi \in \mathcal{R}$. In line 1 of expression (7), the normalizing constant $(1 - \sum_{v=1}^{\infty} \varpi_v^T)$ is the total probability that a T -variate random vector whose elements are i.i.d. G has at least two distinct elements. Then menu distribution W_2 satisfies conditions (i) and (ii), as required. Referring back to the atoms, ζ_v , of distribution G in (5), the list of cuisine 2 dishes is $\mathcal{S}_2 = \{\phi : \phi_t = \zeta_v \text{ for some } v \in \mathcal{N}, \text{ but not all } \phi_t \text{ are identical, } t = 1, \dots, T\}$ and is the support of W_2 . The selection probability associated with a dish ϕ is $W_2(\phi)$.

2.1.1 Restaurant, section, table, and dish choices of the 2R2CF customers

Let the restaurant chosen by franchise customer j be denoted by g_j and the chosen cuisine (i.e., section) be denoted by s_j . Suppose he or she sits at table v_j in that restaurant section and eats dish θ_j .

Customer 1. At time 0, suppose the first customer selects restaurant $g_1 = 1$ with probability $\rho_1 > 0$ and restaurant $g_1 = 2$ with positive probability $\rho_2 = 1 - \rho_1$. For reasons that will become clear, we refer to ρ_1 as the *baseline non-differential proportion* and ρ_2 as the *baseline differential proportion*. Typically, the differential state is relatively less frequent, and so $\rho_2 < \rho_1$ (i.e., $\rho_2 < 1/2$). Proportion ρ_1 is given a uniform prior on the interval $(0.5, 1)$.

Choice of cuisine s_1 Next, customer 1 selects a section in restaurant g_1 . As described earlier, each restaurant specializes in its namesake cuisine, which is therefore more popular with its customers. This is modeled as follows. Within restaurant g_j (where $j = 1$ for the first customer), customer j selects cuisine 1 with probability

$$\mathcal{Q}_{g_j}(1) = \begin{cases} \rho_1 + \rho_2\gamma & \text{if } g_j = 1, \\ \rho_1 - \rho_1\gamma & \text{if } g_j = 2, \end{cases} \quad (8)$$

for a *speciality cuisine popularity parameter*, $\gamma \in (0, 1)$, that determines the degree to which a restaurant's patrons favor its namesake cuisine. For instance, if γ is nearly equal to 1, then a restaurant 1 (2) customer almost always (never) chooses cuisine 1. At the other extreme, if γ is nearly equal to 0, then the customer always chooses cuisine 1 with approximate probability ρ_1 irrespective of the restaurant. Parameter γ is assigned an independent uniform prior on the unit interval. The probability that a restaurant g_j customer chooses cuisine 2 is then $\mathcal{Q}_{g_j}(2) = 1 - \mathcal{Q}_{g_j}(1)$.

Choice of table v_1 and dish θ_1 Within section s_1 of restaurant g_1 , since the table identifiers are arbitrary, we assume without loss of generality that customer 1 sits at table $v_1 = 1$. As the 2R2CF process evolves, the tables in a restaurant's section are assigned consecutive labels as newly arriving patrons occupy them. At table $v_1 = 1$, customer 1 randomly orders a cuisine s_1 dish from menu distribution W_{s_1} . The dish he or she eats represents the random effect of the first probe. That is, $\theta_1 \mid s_1 \sim W_{s_1}$.

Customer j , for $j > 1$. The *restaurant* choice of a subsequent customer is influenced by the previous customer's *cuisine* and the waiting time between the customers. Suppose customer j arrives at the franchise after a time interval of e_{j-1} following the $(j - 1)$ th customer. Without loss of generality, e_1, \dots, e_{p-1} are scaled so that their total equals 1. Since the probes in differential analysis typically represent CpG sites on a chromosome or gene, it has a scaled length of 1.

To model the dependencies between the franchise customers, we first define a non-negative **dependence parameter** η that transforms the waiting time e_{j-1} to an **affinity** measure between customer $(j - 1)$ and customer j :

$$r_j = \exp(-e_{j-1}/\eta), \quad j > 1. \quad (9)$$

The affinity measure belongs to the unit interval when $\eta > 0$. If $\eta = 0$, affinity r_j is defined as 0 irrespective of the waiting time. The affinity influences the behavior of customer j through equation (10) below.

Choice of restaurant g_j The cuisine s_{j-1} of the $(j - 1)$ th customer influences the

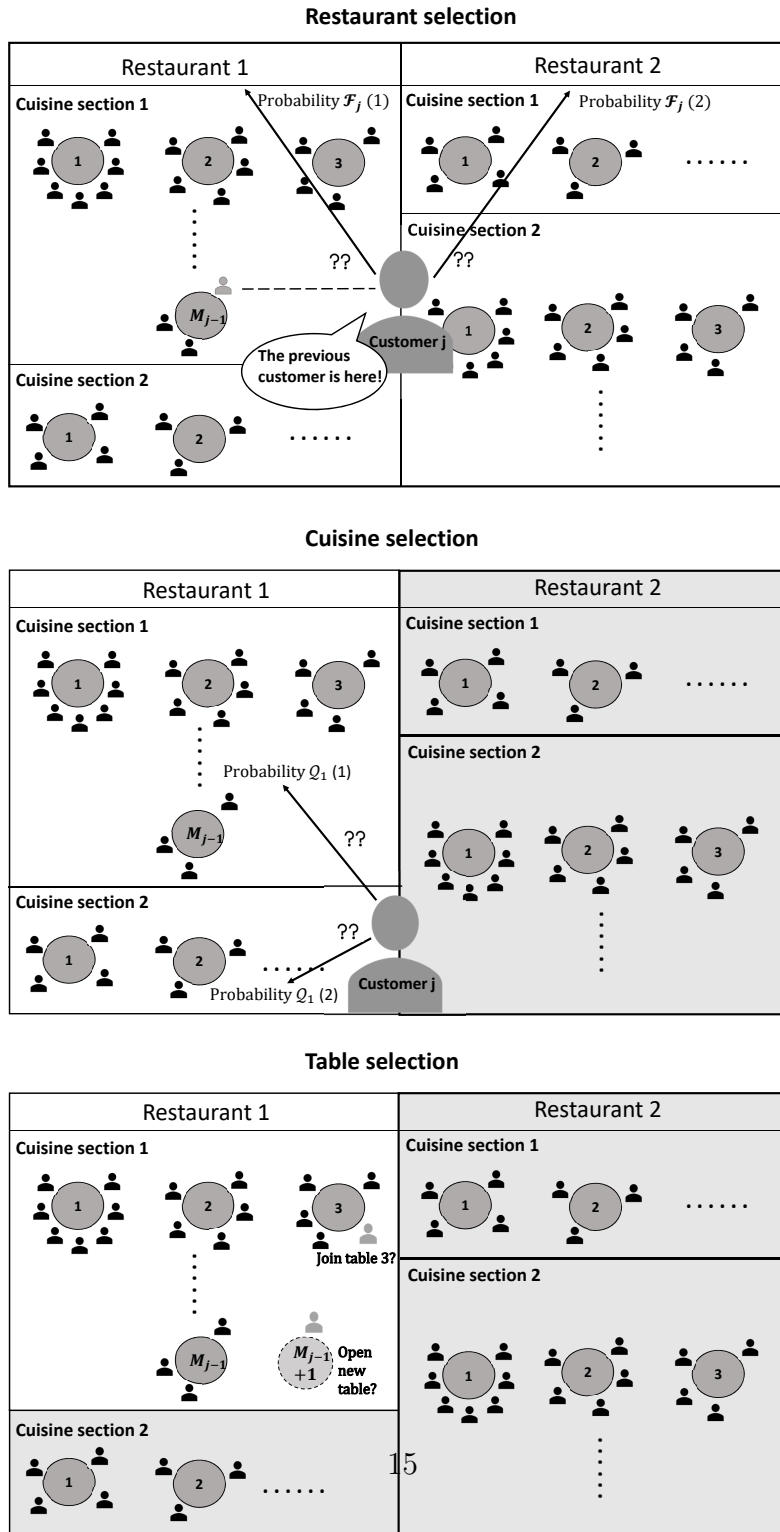


Figure 2: Cartoon representation of the two-restaurant two-cuisine franchise for differential analysis, showing the progressive choice of restaurant, cuisine section, and table by customer j , for $j > 1$. The numbered circles represent table numbers. See the text in Section 2.1 for a detailed description of the process.

restaurant choice of the j th customer through affinity r_j and popularity parameter γ :

$$g_j \mid s_{j-1}, \rho_1, \eta, \gamma \sim \mathcal{F}_j.$$

Specifically, the probability that customer j selects restaurant 1 is assumed to be

$$\mathcal{F}_j(1) \stackrel{def}{=} P(g_j = 1 \mid s_{j-1}, \rho_1, \eta, \gamma) = \begin{cases} \rho_1 + \rho_2 r_j / \gamma & \text{if } s_{j-1} = 1, \\ \rho_1 - \rho_1 r_j / \gamma & \text{if } s_{j-1} = 2, \end{cases} \quad (10)$$

and $\mathcal{F}_j(2) = 1 - \mathcal{F}_j(1)$. If dependence parameter $\eta = 0$, we find that the restaurant choices of the customers are independent; specifically, $\mathcal{F}_j(1) = \rho_1$ irrespective of the cuisine s_{j-1} . The idea is illustrated in the top panel of Figure 2, where customer j chooses restaurant 1 with probability $\mathcal{F}_j(1)$ and restaurant 2 with probability $\mathcal{F}_j(2)$.

It can be verified that \mathcal{F}_j is a probability mass function if and only if $r_j/\gamma < 1$. Since the scaled waiting times are bounded above by 1, a globally sufficient condition is $\eta < -1/\log \gamma$. We, therefore, assume a mixture prior for dependence parameter η :

$$\eta \mid \gamma \sim \frac{1}{2}\delta_0 + \frac{1}{2}\mathcal{H} \cdot \mathcal{I}(\eta < -1/\log \gamma), \quad (11)$$

where the second mixture component involves a continuous distribution, \mathcal{H} , restricted to the interval $[0, -1/\log \gamma)$, thereby enforcing the globally sufficient condition. In our experience, posterior inferences on η are relatively robust to the continuous prior \mathcal{H} provided the prior is not highly concentrated on a small part of interval $[0, -1/\log \gamma)$.

When $\eta = 0$, we have a *zero-order Sticky PYP*; when $\eta > 0$, we obtain a *first order Sticky PYP*. Some interesting consequences of specification (10) are:

1. **Zero-order Sticky PYP:** When $\eta = 0$, each customer independently chooses restaurant 1 (or 2) with a baseline probability of ρ_1 (or ρ_2). The p customers act identically.
2. **First order Sticky PYP with e_{j-1}/η large:** At large relative distances, customer j acts approximately independently of the history. Somewhat similarly to customer 1, customer j chooses restaurant 1 (2) with a probability approximately, but not exactly, equal to ρ_1 (ρ_2).

3. **First order Sticky PYP with e_{j-1}/η small:** In the limit as $e_{j-1}/\eta \rightarrow 0$ (e.g., for a small inter-probe distance e_{j-1}), the restaurant choice of customer j follows a hidden Markov model.

Since it drives the dependence characteristics of DNA methylation data, parameter η is of interest. Prior specification (11) allows the data to direct the model order through posterior probability, $P[\eta = 0 \mid \mathbf{X}]$, and an MCMC probability is readily available.

Choice of cuisine s_j Upon entering restaurant g_j , customer j selects cuisine-section s_j with distribution \mathcal{Q}_{g_j} , defined previously in expression (8). For bookkeeping reasons, among franchise customers $1, \dots, j$, suppose $p_{gs}^{(j)}$ customers choose section s in restaurant g ; that is, $p_{gs}^{(j)} = \sum_{l=1}^j \mathcal{I}(g_l = g, s_l = s)$ for $g, s = 1, 2$.

For a graphical depiction of cuisine selection by the j th customer, see the middle panel of Figure 2, where $g_j = 1$. That is, customer j , having already chosen restaurant 1, now chooses a cuisine-section. Restaurant 2 has been greyed out because it is no longer accessible to this customer. In the lower panel of Figure 2, we find that the customer picked cuisine-section 1, so that $s_j = 1$.

Choice of table v_j Applying the above notation, among the previous customers $1, \dots, (j-1)$, there are $p_{g_j s_j}^{(j-1)}$ customers in the same restaurant and section as the j th customer. Suppose these customers have occupied tables $1, \dots, M_{g_j s_j}^{(j-1)}$, and that there are $p_{g_j s_j k}^{(j-1)}$ customers seated at the k th table. Let $\mathcal{M}_{j-1} = \{p_{g_j s_j k}^{(j-1)} : k = 1, \dots, M_{g_j s_j}^{(j-1)}\}$ denote the aggregated table occupancies.

Recall that the newly arrived j th customer may sit at any of the $M_{g_j s_j}^{(j-1)}$ occupied tables or a new $(M_{g_j s_j}^{(j-1)} + 1)$ th table. Two possibilities are illustrated in the lower panel of Figure 2. For a PYP with mass parameter α_{s_j} and cuisine-specific discount parameter $d_{s_j} \in [0, 1)$, the predictive distribution of table v_j of customer j is assumed to be related to the table occupancies:

$$P\left(v_j = k \mid \mathcal{M}_{j-1}\right) \propto \begin{cases} p_{g_j s_j k}^{(j-1)} - d_{s_j} & \text{if } k = 1, \dots, M_{g_j s_j}^{(j-1)}, \\ \alpha_{s_j} + M_{g_j s_j}^{(j-1)} d_{s_j} & \text{if } k = (M_{g_j s_j}^{(j-1)} + 1), \end{cases} \quad (12)$$

where the second line corresponds to customer j sitting at a new table, in which case the new number of occupied tables is $M_{g_j s_j}^{(j)} = M_{g_j s_j}^{(j-1)} + 1$ and table index $v_j = M_{g_j s_j}^{(j)}$. Otherwise,

if customer j sits at a previously occupied table, then their table index $v_j \leq M_{g_j s_j}^{(j-1)}$ and the number of occupied tables remains unchanged: $M_{g_j s_j}^{(j)} = M_{g_j s_j}^{(j-1)}$.

The above predictive distribution implies that customer j is more likely to choose tables with several occupants, positively reinforcing that table's popularity for future customers. The number of occupied tables stochastically increases with the PYP mass and discount parameters.

For section s , if the PYP discount parameter $d_s = 0$, we obtain the well-known Pòlya urn scheme for Dirichlet processes (Ferguson 1973b). PYPs act as effective dimension reduction devices because the random number of occupied tables is much smaller than the number of customers. In general, as the number of patrons in section s of restaurant g grows as more customers arrive at the franchise, that is, as $p_{gs}^{(j)} \rightarrow \infty$, the number of occupied tables, $M_{gs}^{(j)}$, is asymptotically equivalent to

$$\begin{cases} \alpha_s \log p_{gs}^{(j)} & \text{if } d_s = 0 \\ T_{d_s \alpha_s} p_{gs}^{(j)} & \text{if } 0 < d_s < 1 \end{cases} \quad (13)$$

for a positive random variable $T_{d_s \alpha_s}$ (Lijoi & Prünster 2010). Asymptotically, the order of the number of occupied tables increases with discount parameter d_s .

Choice of dish θ_j As we have discussed earlier, the 2R2CF process assumes that all customers seated at a table of section s_j are served the same dish, chosen from the cuisine s_j menu by the first customer to sit at that table. Let $\phi_{g_j s_j k}$ denote the common dish eaten by the previous $(j-1)$ customers at the k th table, $k = 1, \dots, M_{g_j s_j}^{(j-1)}$.

Following predictive distribution (12), if customer j has chosen to sit at a previously occupied table, then she or he is served the dish selected by the first customer to sit at that table. Otherwise, if customer j has chosen a new table, then she or he randomly picks a dish from menu distribution W_{s_j} . The dish that customer j eats represents the probe-specific random effect θ_j , and

$$\theta_j \begin{cases} = \phi_{g_j s_j v_j} & \text{if } v_j = 1, \dots, M_{g_j s_j}^{(j-1)}, \\ \sim W_{s_j} & \text{if } v_j = (M_{g_j s_j}^{(j-1)} + 1). \end{cases} \quad (14)$$

In the latter case (line 2), the dish θ_j randomly selected by customer j is registered as $\phi_{g_j s_j M_{g_j s_j}^{(j)}}$ and is served to all future customers who sit at table $M_{g_j s_j}^{(j)}$. Assumptions (12) and (14) imply that although the restaurants serve the same menus, the relative popularity of each dish is restaurant-specific.

The aforementioned process continues for the remaining 2R2CF customers. Expressions (8) and (10) guarantee that a cuisine is more popular at its namesake restaurant and the cuisine selected by a customer influences the restaurant choice of the next customer, making the next customer likely to select the same cuisine. This accounts for the lengthy runs of differential or non-differential probes observed in methylation data. In addition to achieving dimension reduction, the proposed Sticky PYP models the serial dependencies of adjacent probes as a decreasing function of the inter-probe distances.

2.1.2 Latent clusters and their differential states

Latent clusters, introduced earlier in expression (3), comprise probes with identical random effects and form the basis of the dimension reduction strategy. Returning to the 2R2CF metaphor, we identify a cluster as the set of customers who eat the same dish. However, in addition to the customers seated at a table, multiple tables in both restaurants may serve the same dish because of the shared cuisine menu. Therefore, irrespective of the restaurant, aggregating customers eating the same dishes, we obtain the probe-cluster allocation variables c_1, \dots, c_p , and the number of latent clusters, q . The sets of customers eating the same cuisine 2 (differential state) dishes correspond to the differential clusters, \mathcal{D} , defined in equation (4).

From expression (13), we expect the number of occupied tables to be much smaller than the number of franchise customers, p . Furthermore, since multiple tables may serve the same dish, we expect the number of latent clusters, q , to be smaller than the number of occupied tables. With high probability, this implies that q is much smaller than p .

PYP discount parameter d_2 . Consider the differential state cuisine menu, W_2 , defined in (7). It can be shown that as the number of treatments, T , and the number of probes, p , increase, the differential clusters are not only asymptotically identifiable but consistently

detectable in the posterior; refer to Section 4 of [Guha & Baladandayuthapani \(2016\)](#) for a detailed general discussion of this remarkable phenomenon in standard PYP settings. Since the differential clusters can be inferred with high accuracy when T and p are large, discount parameter d_2 is given the mixture prior:

$$d_2 \sim \frac{1}{2}\delta_0 + \frac{1}{2}U(0, 1)$$

where $d_2 = 0$ corresponds to a Dirichlet process. This provides the posterior flexibility to choose between a Dirichlet process and a more general PYP for a suitable clustering pattern of the differential probes. Allocation patterns typical of Dirichlet processes, such as exponentially decaying cluster sizes dominated by a few large clusters, result in high posterior probabilities that d_2 equals 0. By contrast, allocation patterns characteristic of non-Dirichlet PYPs, such as slower-than-exponential power law decays in the cluster sizes and relatively large numbers of smaller-sized clusters, cause the posterior of discount parameter d_2 to concentrate near 1 and exclude 0. A proof of the intrinsically different cluster patterns of Dirichlet processes and PYPs is given in Theorem 2.1 of [Guha & Baladandayuthapani \(2016\)](#).

Since distribution G is discrete, all atoms of T -variate distribution W_2 may not be unique. Indeed, this is common for $T = 2$ treatments. However, as T grows, and provided the number of probes, p , grows at a slower-than-exponential rate as T , the probability that two atoms allocated to the probes are identical rapidly decays to 0. In regression problems unrelated to differential analysis, Section 2.3 of [Guha & Baladandayuthapani \(2016\)](#) derived a similar result for a simpler zero-order stochastic process. We have verified this phenomenon in simulation studies on differential analysis datasets. In several hundred artificial datasets generated from the Sticky PYP, for $p = 1,500$ probes and T as small as four, no two allocated atoms of W_2 were identical.

PYP discount parameter d_1 . Consider the (non-differential) cuisine menu, W_1 , defined in (6). The flexibility provided by PYP allocation patterns is not necessary for the non-differential probes. This is because the allocation patterns of distribution W_1 are driven by univariate parameter ψ in (6), and, in general, the mixture allocations of univariate

objects are unidentifiable (e.g., [Frühwirth-Schnatter 2006](#)). Consequently, we set PYP discount parameter $d_1 = 0$, reducing the two PYPs associated with the non-differential state (i.e., section 1 in both restaurants) to Dirichlet processes.

2.1.3 Other model parameters

Depending on the specifics of the application, an appropriate model is assumed for the subject-specific parameters ξ_1, \dots, ξ_n . For example, we may assume that $\xi_i \stackrel{iid}{\sim} N(0, \tau_\epsilon^2)$. In some applications, it is more appropriate to assume non-zero means and flexible error distributions: $\xi_i = b_i + \epsilon_i$, where b_i represents lane or batch effects in methylation data, and the i.i.d. ϵ_i have a random distribution with a Dirichlet process prior whose normal base distribution has mean zero and variance τ_ϵ^2 . Similarly, appropriate models for the probe-specific parameters χ_1, \dots, χ_p may include i.i.d. zero-mean normal distributions, and finite mixtures or HMMs with state-specific normal distributions. Inverse-gamma priors are assigned to σ^2 and τ_ϵ^2 . Appropriate priors are assumed for mass parameters β , α_1 , and α_2 in expressions (6) and (12). Mean μ_G and variance τ_G^2 of base distribution G_0 in expression (6) are given a joint normal-inverse gamma prior. Figure 11 of Supplementary Materials displays a directed acyclic graph summarizing the relationships between the different BayesDiff model parameters.

3 Posterior Inference

Due to the analytical intractability of the BayesDiff model, we rely on MCMC methods for posterior inferences and detection of differential probes.

3.1 MCMC Strategy

The model parameters are initialized using naïve estimation techniques and iteratively updated by MCMC techniques until the chain converges. We split the MCMC updates into three blocks. An outline of the MCMC procedure is as follows. Further details can be found in Section 7 of Supplementary Material.

1. **Restaurant-cuisine-table-dish choice** $(g_j, s_j, v_j, \boldsymbol{\theta}_j)$ **of customer j** : For each probe $j = 1, \dots, p$, we sample the 4-tuple $(g_j, s_j, v_j, \boldsymbol{\theta}_j)$ given the 4-tuples of the other $(p-1)$ probes. This is achieved by proposing a new value of $(g_j, s_j, v_j, \boldsymbol{\theta}_j)$ from a carefully constructed approximation to its full conditional, and by accepting or rejecting the proposed parameters in a Metropolis-Hastings step. The procedure is repeated for all p probes. As discussed in Section 2.1.2, the probe-cluster allocations c_1, \dots, c_p are immediately available from the restaurant-cuisine-table allocations (g_j, s_j, v_j) of the p probes. Also available are the q latent clusters along with their allocated probes, and the set of differential clusters \mathcal{D} .
2. **Latent vectors** $\boldsymbol{\lambda}_1, \dots, \boldsymbol{\lambda}_q$: There are Tq latent vector elements, not all of which are necessarily distinct because of the Dirichlet process prior on distribution G . Although the latent vector elements are known from the Block 1 updates, MCMC mixing is considerably improved by updating the latent vector elements conditional on the p probe-cluster allocations. As the calculation in Supplementary Material shows, this is possible by Gibbs sampling.
3. **Remaining model parameters**: Generated by standard MCMC techniques.

For the numerical analyses of this paper, we discarded an initial burn-in of 10,000 MCMC samples and used the subsequent 50,000 draws for posterior inferences. Convergence was informally assessed by trace plots of various hyperparameters to validate the MCMC sample sizes. For the proposed moves (in discrete parameter space) described in Step 1, the average Metropolis-Hastings acceptance rate exceeded 90% in all our analyses.

3.2 Detection of Differential Probes with FDR Control

Post-processing the MCMC sample, a Bayesian approach for controlling the false discovery rate (FDR) (Newton et al. 2004) is applied to accurately detect the probes j with differential state $s_j = 2$. Specifically, let q_0 be the nominal FDR level and ω_j be the posterior probability that probe j is differential, so that $\omega_j = P[s_j = 2 \mid \mathbf{X}]$. An empirical average estimate, $\hat{\omega}_j$, is available from the MCMC sample. To achieve the desired FDR level in

calling the differential probes, we first rank all the probes in decreasing order of $\hat{\omega}_j$. Let $\hat{\omega}_{(1)} > \hat{\omega}_{(2)} > \dots > \hat{\omega}_{(p)}$ denote the ordered posterior probability estimates. For each $b = 1, \dots, p$, we calculate as follows the posterior expected FDR resulting from calling the first b probes in decreasing order of $\hat{\omega}_j$:

$$\widehat{\text{FDR}}_b = \frac{\sum_{j=1}^p (1 - \hat{\omega}_j) \mathcal{I}(\hat{\omega}_j \geq \hat{\omega}_{(b)})}{\sum_{j=1}^p \mathcal{I}(\hat{\omega}_j \geq \hat{\omega}_{(b)})} = \frac{\sum_{j=1}^b (1 - \hat{\omega}_{(j)})}{b}, \quad (15)$$

where the simplification occurs because the $\hat{\omega}_j$'s are sorted. Finally, we pick the largest value of b , denoted by b^* , for which $\widehat{\text{FDR}}_{b^*} < q_0$. A nominal FDR level of q_0 is achieved by labeling as differential the first b^* probes arranged in decreasing order of $\hat{\omega}_j$.

4 Simulation Studies

Using artificial datasets with $T = 5$ treatments, we analyzed the accuracy of BayesDiff in detecting differentially methylated probes. We also compared the results with established differential methylation procedures and general statistical techniques for multiple treatment comparisons. Further, we evaluated the ability of the BayesDiff procedure in discovering the complex dependence structure of DNA methylation data.

Generation strategy Proportions representing DNA methylation data were generated using the logit transformation as in equation (1). The inter-probe distances were the actual distances from the motivating TCGA dataset, scaled to add to 1. In order to capture the complexity of methylation data, such as the existence of multiple latent methylation states (e.g., CpG islands and shores), different read depths across CpGs, and the incomplete conversion of bisulphite sequencing, the generation strategy was partly based on techniques implemented in WGBSSuite, a flexible stochastic simulation tool for generating single-base resolution methylation data (Rackham et al. 2015). However, the generation procedure differed from WGBSSuite in some respects. Specifically, it allowed more than two treatments ($T > 2$). Additionally, as in actual methylation datasets, the generation procedure incorporated serial dependence not only in the methylation levels but also in the differential states of the probes.

The probes-specific read depths were generated as $n_j \stackrel{iid}{\sim} \text{Poisson}(50)$. Unlike BayesDiff assumption (1), there were no subject-specific random effects in the generation mechanism. Instead, the normal mean of the generated data included additive probe-specific random effects, $\chi_1^{(0)}, \dots, \chi_p^{(0)}$, that were generated as follows:

1. Generate the true methylation status of the probes, denoted by $h_1^{(0)}, \dots, h_p^{(0)}$, using the 4-state *distance-based* HMM of Rackham et al. (2015), with the states respectively representing the methylated, first transit, demethylated, and second transit states.
2. Set the baseline methylation levels for the methylated, (first or second) transit, and demethylated states as $p_{\text{methylated}} = 0.8$, $p_{\text{transit}} = 0.5$, and $p_{\text{un-methylated}} = 0.2$.
3. For $j = 1, \dots, p$, define the mean probe-specific random effect as follows:

$$\tilde{\chi}_j^{(0)} = \begin{cases} \log\left(\frac{p_{\text{methylated}}}{1-p_{\text{methylated}}}\right) & \text{if } h_j = 1 \text{ (i.e., methylated state),} \\ \log\left(\frac{p_{\text{transit}}}{1-p_{\text{transit}}}\right) & \text{if } h_j = 2, 4 \text{ (first or second transit state),} \\ \log\left(\frac{p_{\text{demethylated}}}{1-p_{\text{demethylated}}}\right) & \text{if } h_j = 3 \text{ (i.e., demethylated state).} \end{cases}$$

4. Independently generate true probe-specific random effects: $\chi_j^{(0)} \sim N(\tilde{\chi}_j^{(0)}, \tau_\chi^2)$ for probe $j = 1, \dots, p$.

Noise and dependence levels We investigated four scenarios corresponding to the combinations of two noise levels and two dependence levels. For each scenario, 20 datasets were independently generated, with each dataset consisting of $p = 500$ probes and $T = 5$ treatments with 4 samples each, i.e., a total to $n = 20$ samples. The low noise level corresponded to true variance parameter $\sigma_0^2 = 0.36$; equivalently, to a signal-to-noise of $R_0^2 \approx 70\%$. The high noise level corresponded to $\sigma_0^2 = 1$ or $R_0^2 \approx 40\%$. The true between-probe dependencies comprised two levels: no serial correlation (i.e., a zero-order Sticky PYP) with $\eta_0 = 0$, and positive serial correlation (i.e., a first order Sticky PYP) with $\eta_0 = 0.004$. Although $\eta_0 = 0.004$ may appear to be small, its value is calibrated to the inter-probe distances; when the distance between two adjacent probes is equal to the standardized

α_1	α_2	d_2	β	γ	ρ_2	μ_G	τ_G^2	τ_χ^2
20	20	0.33	20	0.9	0.1	0	1	0.1225

Table 1: True parameter values used to generate the artificial datasets.

average distance of $\bar{e} = 1/(p - 1) = 1/499$, $\eta_0 = 0.004$ gives an affiliation of $r_0 = 0.6$ in equation (9). Since the affiliations are bounded above by 1, $\eta_0 = 0.004$ represents fairly high inter-probe dependence. For convenience, we will refer to the two dependence levels as “no-correlation” and “high correlation.” The other model parameters were common for the four scenarios and are displayed in Table 1. Setting a true baseline differential proportion of $\rho_2 = 0.1$ resulted in approximately 10% true differentially methylated CpGs in each dataset.

Posterior inferences Assuming all model parameters to be unknown, each artificial dataset was analyzed using a BayesDiff model that differed in key respects from the true generation mechanism. For example, unlike the 4-state HMM of the generation strategy, the probe-specific random effects χ_j were analyzed using a BayesDiff model that ignored the first order dependence, and instead, relied on a 3-state finite mixture model representing the methylated, transit, and unmethylated states. Additionally, in contrast to the zeroed-out subject-specific random effects during data generation, the BayesDiff procedure assumed that the random effects were i.i.d. normal with zero mean.

To assess the accuracy of BayesDiff in detecting the absence or presence of inter-probe serial correlation, in the no-correlation ($\eta_0 = 0$) situation, we evaluated $\log \left(\frac{P[\eta=0|\mathbf{X}]}{P[\eta>0|\mathbf{X}]} \right)$, the log-Bayes factor comparing zero order to first order Sticky PYPs. In the high correlation ($\eta_0 = 0.004$) situation, we evaluated $\log \left(\frac{P[\eta>0|\mathbf{X}]}{P[\eta=0|\mathbf{X}]} \right)$, the log-Bayes factor comparing first order to zero order Sticky PYPs. Thus, in any scenario, a large positive value of this measure constitutes strong evidence that BayesDiff detects the correct model order.

Although conceptually straightforward, the estimation of Bayes factors requires multiple MCMC runs even for relatively simple parametric models (Chib 1995). Basu & Chib (2003) extended the estimation strategy to infinite dimensional models such as Dirichlet

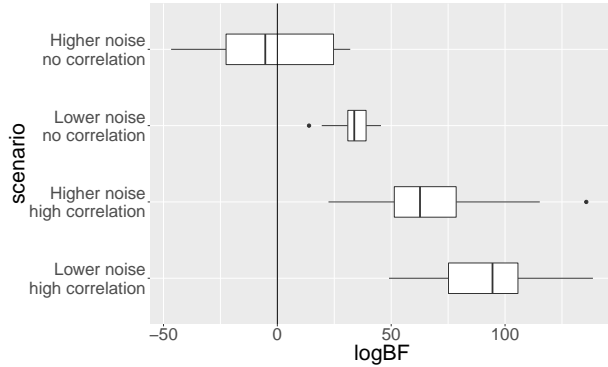


Figure 3: Simulation study box plots for estimated lower bounds of log-Bayes factors in favor of the true model order.

processes. However, the computational costs are prohibitively high for big datasets, and multiple MCMC runs for estimating Bayes factors would stretch available computational resources beyond their present-day limits. Faced with these challenges, we relied on an alternative strategy for estimating the *lower bounds* of log-Bayes factors using a single MCMC run. As it turns out, this is often sufficient to infer the Sticky PYP model orders. Let Θ^- denote all BayesDiff model parameters except η . In the high correlation situation, applying Jensen’s inequality, a lower bound for the corresponding log-Bayes factor is $E \left[\log \left(\frac{P[\eta > 0 | \mathbf{X}, \Theta^-]}{P[\eta = 0 | \mathbf{X}, \Theta^-]} \right) \mid \mathbf{X} \right]$. Unlike log-Bayes factors, this lower bound can be easily estimated by an empirical average estimate based on a single MCMC run. In the no-correlation situation, a lower bound for the log-Bayes factor, $\log \left(\frac{P[\eta = 0 | \mathbf{X}]}{P[\eta > 0 | \mathbf{X}]} \right)$, can be similarly derived.

For each of the four generation scenarios, box plots of these estimated lower bounds for the 20 datasets are depicted in Figure 3. Except for the high noise–no-correlation scenario, for which the results were inconclusive, the estimated lower bounds of the log-Bayes factors in favor of the true correlation structure were all positive and large. In the low noise–no-correlation scenario, BayesDiff decisively favored zero-order models, and the smallest lower bound among the 20 datasets was 13.9, corresponding to Bayes factors exceeding $e^{13.9} = 1,088,161$. The 25th percentile of these lower bounds was 30.9, corresponding to Bayes factors exceeding $e^{30.9} = 2.63 \times 10^{13}$. This is strong evidence that the BayesDiff

approach is reliable in this scenario. For the high-correlation scenarios, the estimated lower bounds were even higher, showing that BayesDiff overwhelmingly favors first order models when the data are actually serially correlated.

Comparisons with other methods We evaluated the success of the BayesDiff procedure in detecting disease genomic signatures and made comparisons with six well-known procedures. These included some general statistical techniques for multiple treatment comparisons, namely, one-way analysis of variance (ANOVA) and the Kruskal-Wallis test. We also made comparisons with some methods specially developed for detecting differential methylation in more than two treatments: COHCAP ([Warden et al. 2013](#)), methylKit ([Akalin et al. 2012](#)), BiSeq ([Hebestreit et al. 2013](#)), and RADMeth ([Dolzhenko & Smith 2014](#)). The ANOVA and Kruskal-Wallis test procedures were applied separately on each probe after applying the inverse-logit transform. Being specifically designed for differential methylation analysis, the COHCAP method was directly applied to the generated proportions of the synthetic data. The remaining three methods are designed for bisulfite sequencing, which consists of the total methylation reads for each measured CpG site. For these methods, the methylation reads for each probe was obtained by multiplying the proportion methylation values by the total read. The bandwidth smoothing parameter of the method BiSeq was tuned to optimize the overall detection. For all six methods, probe-specific p-values were evaluated and adjusted for multiplicity using the FDR control procedure of [Benjamini & Hochberg \(1995\)](#).

As with most nonparametric Bayes techniques, the associated computational costs of BayesDiff are considerably higher compared to frequentist methods. However, the additional run times are negligible compared to the time frames over which the experimental data are collected, and as we demonstrate, the trade-off is the substantially greater accuracy achieved by BayesDiff. On a personal computer with an Intel Core i7-4770 processor with 3.40 GHz frequency and 8 GB RAM, the average computational time for the [Section 3.1](#) MCMC algorithm, for the $n = 20$ samples, $T = 5$ treatments, and $p = 500$ probes of the simulation study datasets, was 0.60 seconds per iteration. The computational times were reduced when different simulation datasets were run in parallel across multiple cores of a

research computing cluster. Analyzing datasets of different sizes, we find that the computational cost is $O(Tp^2)$ but does not appreciably depend on n/T . This is reasonable because the mixture model primarily focuses on $\theta_1, \dots, \theta_p \in \mathcal{R}^T$. Due to the intensive nature of the one-parameter-at-a-time Gibbs sampling updates in Block 2, the Metropolis-Hastings algorithm of Guha (2010) can be applied to significantly speed up the updates and make the calculations more scalable. As part of ongoing development of a fast R package, we find that ten- to hundred-fold speedups are possible with this fast MCMC strategy, which can also be applied to quickly generate the Block 1 parameters.

We computed the receiver operating characteristic (ROC) curves for differential probe detection for all seven methods. For a quantitative assessment, we calculated the area under curve (AUC), declaring the method with the largest AUC as the most reliable in each scenario. The ROC curves, averaged over the 20 datasets under each simulation scenario, are shown with the AUCs in Figure 7 of Supplementary Material. In all except the high-noise–no-correlation scenario, BayesDiff uniformly outperformed the other methods. Even in the high-noise–no-correlation scenario, BayesDiff performed better in the low FPR region. As expected, all seven methods had lower accuracies for higher noise levels. BayesDiff did significantly better than the competing methods in the high correlation scenarios, suggesting that the incorporation of between-probe dependencies improves its accuracy in situations typical of DNA methylation data.

Since researchers typically focus on small false positive rates (FPRs), that is, small significance levels, we also calculated the measures, AUC_{20} and AUC_{10} . AUC_{20} (AUC_{10}) is defined as the area under the ROC curve multiplied by 5 (10) when the FPR does not exceed 0.2 (0.1). The multiplicative factor ensures that the areas potentially vary between 0 and 1. The three versions of AUC are presented in Table 3 in Supplementary Material. As also seen in Figure 7, Table 3 reveals that in three of the four scenarios, BayesDiff had the largest overall AUC. Furthermore, BayesDiff had vastly improved reliability for low FPRs. For example, consider the low noise–high correlation scenario. The overall AUC for BayesDiff was 0.035 greater than that for ANOVA. In contrast, the gains for BayesDiff, relative to ANOVA, were +0.107 for AUC_{20} and +0.146 for AUC_{10} . The advantages of BayesDiff were even greater relative to the other competing methods. In the high noise–

low-correlation scenario, BayesDiff had a relatively low AUC, as mentioned. However, even in this scenario, it had the greatest AUC_{20} and AUC_{10} values among all the methods. Additionally, for a nominal FDR level of $q_0 = 0.05$, the achieved FDR of BayesDiff was between 0 and 0.03 in every dataset and simulation scenario. These results demonstrate the ability of BayesDiff to accurately detect the differential probes even in challenging situations where the FPR is small.

5 Data Analysis

We returned to the motivating DNA methylation dataset consisting of the upper GI cancers: stomach adenocarcinoma (STAD), liver hepatocellular carcinoma (LIHC), esophageal carcinoma (ESCA) and pancreatic adenocarcinoma (PAAD). Applying the BayesDiff procedure, we detected the differentially methylated CpG loci among the cancer types.

Data processing The dataset was obtained from The Cancer Genome Atlas project, publicly available through The Genomic Data Commons (GDC) portal ([Grossman et al. 2016](#)). The data are available from the Illumina Human Methylation 450 platform for each of 485,577 probes at the CpG sites. At the time of analysis, the dataset consisted of 1,224 tumor samples. The analysis was performed on a gene-by-gene basis. We picked a set of 443 genes involving mutation in at least 5% of the samples. To ensure that all CpG sites potentially related to a gene were included in the analysis, we selected all sites located within 50K base pairs outside the gene body, specifically, upstream from the 5' end and downstream from the 3' end. The number of gene-specific CpG sites ranged from 1 to 769, and are displayed in Figure 8(a) of Supplementary Material. As a final preprocessing step, since the methylation patterns of short genes are of less interest in cancer investigations, we eliminated the 25 genes mapped to 20 or fewer CpG sites.

Inference procedure The data were analyzed using the proposed BayesDiff approach. Exploratory analyses indicated that a satisfactory fit was obtained by eliminating the probes-specific random effects χ_j in (1). Since information about experimental batches is

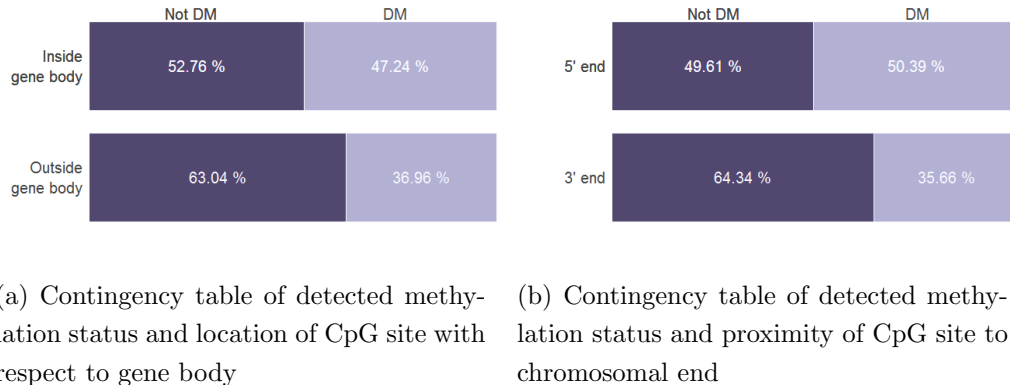


Figure 4: Associations of detected methylation status and position of CpG sites.

not available for the TCGA dataset, we assumed that the i.i.d. ξ_1, \dots, ξ_n parameters follow a random distribution with a zero-mean Dirichlet process prior. The MCMC procedure of Section 3.1 was applied to obtain posterior samples for each gene. For detecting differential CpG sites, we applied the Section 3.2 procedure with a nominal FDR of $q_0 = 0.05$.

Results Among the differentially methylated CpG sites detected by our approach, approximately 40.6% of the sites were located outside the gene bodies. Figure 4 displays the associations between detected methylation status and positions of the CpG sites. For our analysis, we have defined “near the 5’ (3’) end” as the CpG sites located within one-fourth length of the gene body, either inside or outside the gene boundary, and closer to the transcription start (termination) site. Our results indicate that the proportion of differential methylation is higher for CpG sites inside the gene body, and that most differentially methylated loci are situated within the gene body, as is well known from numerous previous studies. However, our analysis also revealed significant amounts of differential methylation outside the gene body. Despite the common belief that DNA methylation analysis should focus on the 5’ end region, we found that CpG sites near the 3’ ends also displayed considerable degrees of differential methylation. These findings support the recommendations of Irizarry et al. (2009) that studies of DNA methylation alteration should be conducted on a higher resolution, epigenome-wide basis.

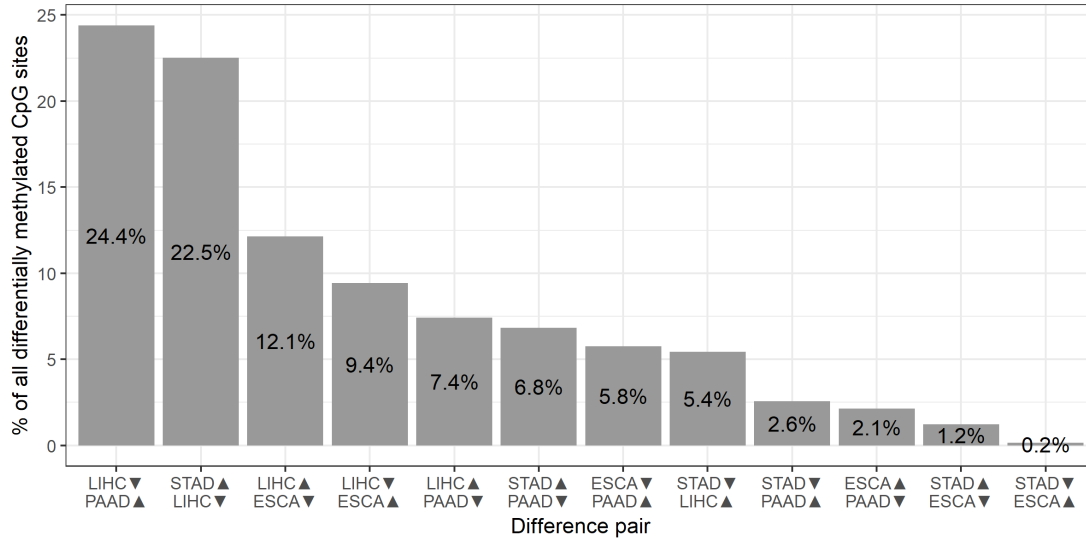


Figure 5: Site-wise summary of the largest pairwise differences of differentially methylated loci among the four upper GI cancer types.

Among the differentially methylated sites detected by BayesDiff, we estimated the pairwise differences between random effects associated with the four cancer types. Site-wise summaries of the largest pairwise differences of the cancer-specific effects are displayed in Figure 5. None of the four cancer types displayed consistent hypermethylation or hypomethylation across all genes or entire chromosomes. However, we found that LIHC is frequently differentially methylated relative to one of the other cancer types, implying that it is the most volatile disease with respect to DNA methylation.

For each gene, Figure 8(b) of Supplementary Material displays 95% credible intervals for lower bounds of log-Bayes factors of a first versus zero-order model, i.e., $\eta = 0$ versus $\eta > 0$ in expression (9). Models with first order dependence are overwhelmingly favored for a majority of the genes, suggesting that statistical techniques that do not account for dependence between neighboring CpG sites would be less effective for these data. Figure 9 of Supplementary Material displays the detailed differential methylation pattern for the top two mutated genes, TP53 and TTN. An obvious feature of both the genes is that the

detected differential methylation of the CpG sites is highly serially correlated. For gene TP53, there are almost no differentially methylated loci within the gene body. The 3' end region outside the gene body has a cluster of differentially methylated loci, for which cancer type STAD is mostly hypermethylated. The results for gene TTN tell a quite different story: most of the differentially methylated loci are inside the gene body and near the 5' end. Cancer type LIHC is hypomethylated compared to PAAD around the 5' end region, but it is hypermethylated compared to STAD near the 3' end. Genes with at least 90% differentially methylated sites detected by BayesDiff are listed in Table 4 of Supplementary Material, along with the largest pairwise difference between the four cancer types among the differentially methylated loci. The number of CpG sites within each segment is listed in Table 5 of Supplementary Material.

Existing medical literature both supports and complements our findings. For example, hypermethylation of the EDNRB and SLIT2 genes have been found in STAD (Tao et al. 2012). Gene FBN2 was hypermethylated in ESCA (Tsunoda et al. 2009). While several studies have found that the gene and protein expressions of ABC transporter genes, such as ABCC9, are useful for understanding the prognosis of esophageal cancer (Vrana et al. 2018), we conclude that hypermethylation of ABCC9 is a major difference between cancer types ESCA and LIHC. Gene FLRT2 is a potential tumor suppressor that is hypermethylated and downregulated in breast cancer (Bae et al. 2017). Our results indicate that this gene is also hypermethylated in cancer type STAD versus LIHC. Mutations in SPTA1 gene has been linked with PAAD (Murphy et al. 2013). Our results indicate that hypermethylation of this gene distinguishes PAAD from LIHC.

Finally, we compared our findings with those of ANOVA for multiple treatment comparisons. Table 6 lists the common set of genes with at least 90% differentially methylated sites identified by both BayesDiff *and* ANOVA. Table 7 displays the genes identified by *only* ANOVA, whereas Table 8 displays the large number of genes detected exclusively by BayesDiff. Cross-referencing with the medical literature, we find that genes FLRT2 and FBN2 were detected by both methods. However, genes EDNRB, SLIT2, ABCC9, and SPTA1 were only identified by BayesDiff, revealing the benefits of the proposed method.

Accounting for data characteristics A statistical model for biomarker data should account for the observed probe-specific means and variances. This is especially important in multiple-testing based approaches where the first two sample moments must be plausibly explained by the fitted model to avoid making misleading biological interpretations (Subramaniam & Hsiao 2012). From this perspective, certain aspects of the BayesDiff model, such as variance σ^2 being a priori unrelated to the mean in expression (1), may appear to be restrictive. However, even though the BayesDiff model was not specifically constructed to match data summaries such as sample moments, in practice, the nonparametric nature of the Sticky PYP allows the posterior to flexibly adapt to the features of the data, including sample moments, thereby accounting for mean-variance relationships in a robust manner. For example, consider again the top mutated genes, TP53 and TTN, discussed in Figure 9 of Supplementary Material. The ability of the BayesDiff model to match the sample moments of the gene-specific probes is demonstrated as follows. Given the inter-probe distances, the joint posterior of the BayesDiff parameters induces predictive distributions on the n measurements for each probe. Functionals of these predictive distributions, such as the probe-specific sample moments, are easily estimated by post-processing the MCMC sample. For these two genes, Figure 10 of Supplementary Material shows that the sample moments predicted by BayesDiff closely match the actual first and second sample moments, with correlations exceeding 99% in each plot. Similar results were observed in other datasets.

6 Discussion

DNA methylation data exhibit complex structures due to unknown biological mechanisms and distance-dependent serial correlations among neighboring CpG sites or probes. The identification of differential signatures among multiple treatments or sets of tumor samples is crucial for developing targeted treatments for disease. This paper formulates a flexible approach applicable to multiple treatments called BayesDiff. The technique relies on a novel Bayesian mixture model called the Sticky PYP or the two-restaurant two-cuisine franchise. In addition to allowing simultaneous inferences on the probes, the model ac-

commodates distance-based serial dependence and accounts for the complex interaction patterns commonly observed in cancer data. A effective MCMC strategy for detecting the differential probes is developed. The success of the BayesDiff procedure in differential DNA methylation, relative to well-established methodologies, is exhibited via simulation studies. The new technique is applied to the motivating TCGA dataset to detect the differential genomic signatures of four upper GI cancers. The results both support and complement various known facts about the epigenomic differences between these cancer types, while revealing a set of genes exhibiting high proportions of differentially methylated CpG sites.

In addition to providing a good fit for the data, a statistical model must be able to account for features of the dataset such as sample moments. The success of the BayesDiff model in this regard is demonstrated in Section 5 for the upper GI dataset. It must be emphasized, however, that there may be datasets where BayesDiff is less successful in accounting for the data characteristics, possibly due to slow asymptotic convergence of the posterior to the true generative process. In such situations, more flexible global transformations (Li et al. 2016) or variance-stabilizing transformations (Durbin et al. 2002) may be used. Alternatively, local Laplace approximations of exponential family likelihoods through link functions (Zeger & Karim 1991, Chib & Winkelmann 2001) may extend the BayesDiff procedure and better explain unique data characteristics.

Like most Bayesian models comprising several latent parameters, the proposed 2R2CF can be marginalized over different parameter sets to obtain equivalent versions of the same model. For example, we could marginalize over the *restaurants* to obtain an equivalent “sticky cuisine” version in which there is just one restaurant with two cuisine-sections and a customer more likely to favor the *cuisine* selected by the previous customer. Alternatively, we could integrate out the *sections* to obtain an equivalent “sticky restaurant franchise” in which each restaurant comprises a single section with restaurant-specific probabilities that guarantee that Cuisine 1 or 2 dishes are more popular at their namesake restaurant; a customer is then more likely to favor the *restaurant* selected by the previous customer. In all equivalent versions, however, a probe’s differential state is determined by the characteristics of the customer’s dish in the metaphor.

The 2R2CF perspective offers the twin advantages of parameter interpretability and

generalizability. Section 9 of Supplementary Material presents the generalized form of the Sticky PYP, revealing the full potential of the proposed method in analyzing not only DNA methylation datasets, but also other types of omics datasets, such as gene expression, RNASeq, and copy-number alteration data. Beyond biomedical applications, the generalized formulation offers a diverse palette of parametric and nonparametric models for capturing the distinctive features of datasets. These Bayesian mixture models are special cases of Sticky PYPs for particular choices of a countable group parameter (e.g., two “restaurants” in the 2R2CF metaphor for differential methylation problems) and countable state parameter (e.g., two “cuisines” in 2R2CF) with the state of a customer influencing the group of the next customer. In addition to extending PYPs to discrete time series type data, the range of models includes Dirichlet processes, PYPs, infinite HMMs, hierarchical Dirichlet processes (Teh et al. 2006), hierarchical Pitman-Yor processes (Teh et al. 2006, Camerlenghi et al. 2019), finite HMMs, nested Chinese restaurant processes (Blei & Jordan 2005), nested Dirichlet processes (Rodriguez et al. 2008), and analysis of densities models (Tomlinson & Escobar 2003).

Ongoing work involves extending the correlation structure to model more sophisticated forms of inter-probe dependence in DNA methylation data. Commented R code implementing the BayesDiff method is available on GitHub at <https://github.com/cgz59/BayesDiff>. Using high-performance Rcpp subroutines, we are developing a fast R package for detecting differential genomic signatures in a wide variety of omics datasets. Initial results indicate that dramatic speedups of several orders of magnitude would allow the fast analyses of high-dimensional datasets on personal computers.

SUPPLEMENTARY MATERIAL

7 MCMC Strategy

As mentioned in Section 3.1 of the paper, we split the MCMC updates into three blocks. The MCMC procedure for updating Blocks 1 and 2 is described below. Unless otherwise stated, all references to equations, tables, and figures are for the main paper.

1. **Restaurant-cuisine-table-dish choice** $(g_j, s_j, v_j, \boldsymbol{\theta}_j)$ **of customer j** : For each probe $j = 1, \dots, p$, we sample the 4-tuple $(g_j, s_j, v_j, \boldsymbol{\theta}_j)$ given the 4-tuples of the other $(p - 1)$ probes. This is achieved by proposing a new value of $(g_j, s_j, v_j, \boldsymbol{\theta}_j)$ from a carefully constructed approximation to its full conditional, and by accepting or rejecting the proposed 4-tuple of probe-specific parameters in a Metropolis-Hastings step. The procedure is repeated for all p probes to complete the block of MCMC updates.

We give here an intuitive description of the details. Further calculation details are available in Section 8 of Supplementary Material. For the j th probe, $1 < j < p$, the choice of restaurant g_j depends on the triplets of the two immediately adjacent probes. Specifically, as discussed in Section 2.1 and graphically shown in the upper and middle panel of Figure 2, the restaurant selected by a customer depends on the cuisine of the previous customer. Then, within restaurant g_j , the customer chooses cuisine s_j with a restaurant-specific probability. Finally, the customer may either sit an existing table, in which case they must eat the same dish as everyone already sitting at that table, or the customer may open a new table and order a dish from cuisine menu s_j . The generation strategy for table and dish depends on the cuisine, as discussed below.

Cuisine $s_j = 1$ Evaluating the posterior probability of table v_j involves integrating the Gaussian likelihood of column vector $\mathbf{z}_j = (z_{1j}, \dots, z_{nj})'$ with respect to the cuisine 1 menu, i.e., $\boldsymbol{\theta}_j \sim W_1$. Recall that the cuisine 1 menu has the special structure (6), allowing its reduction to a univariate quantity distributed as G . This random

distribution itself follows a Dirichlet process conditional prior with a base distribution that is a mixture of known atoms (given the 4-tuples of the other probes) and Gaussian distribution G_0 . This conjugate hierarchical structure allows the calculation of table and dish choice for cuisine 1 in computationally closed form.

Cuisine $s_j = 2$ This situation is more complicated because the Gaussian likelihood must be integrated with respect to prior distribution W_2 of the cuisine 2 dishes. Unlike cuisine 1, this is not possible in computationally closed form because menu structure (7) cannot be reduced to a univariate quantity. In other words, for cuisine 2 (i.e., the differential state), the Dirichlet process conditional prior for distribution G is non-conjugate.

We utilize an auxiliary variable approach. Given the current set and frequency of atoms of distribution G in the other $(p - 1)$ probes, we first compute a finite mixture approximation, G^* , to the Dirichlet process conditional prior for G , as in [Ishwaran & Zarepour \(2002\)](#). Then, using prior (7), it is possible to approximate the posterior probability of customer j joining an existing table or sitting at a new table, irrespective of the dishes. This allows us to generate the table selection, v_j . Finally, we propose the dish, $\theta_j = \phi_{g_j s_j v_j}$. If table v_j is one of the already existing tables, then the customer simply chooses the common, table-specific dish. Otherwise, we sequentially generate from the posterior the T elements representing the new dish. This is done using the corresponding treatment-specific elements of vector $\mathbf{z}_j = (z_{1j}, \dots, z_{nj})'$ and finite mixture G^* , with the restriction that not all T atoms of vector θ_j are equal. The Metropolis-Hasting step compensates for any approximations and produces post-burn-in samples from the BayesDiff model posterior.

Latent clusters As discussed in Section 2.1.2, the probe-cluster allocations c_1, \dots, c_p are immediately available from the restaurant-cuisine-table allocations (g_j, s_j, v_j) of the p probes. The q latent clusters, along with their allocated probes, and the set of differential clusters \mathcal{D} , are also immediately available.

2. **Latent vectors $\lambda_1, \dots, \lambda_q$:** Since each latent vector is of length T , there are Tq latent vector elements, not all of which are necessarily distinct because of the Dirichlet

process prior on distribution G . Although the latent vector elements are available from Block 1, mixing of the MCMC chain is considerably improved by an additional block of updates of the latent vector elements conditional on the p probe-cluster allocations. As the following calculation shows, this can be done by Gibbs sampling. Since a non-differential cluster’s latent vector consists of a single value repeated T times, the number of *distinct* latent vector elements is no more than $(q_1 + Tq_2)$. Given the current probe-cluster allocations, suppose there are m_k probes associated with latent cluster k , where $k = 1, \dots, q$. Let $q_2 = |\mathcal{D}|$ be the number of differential clusters, so that $q_1 = q - q_2$ is the number of non-differential clusters.

Non-differential clusters For these clusters, the latent vector $\boldsymbol{\lambda}_k$ takes the form, $\boldsymbol{\lambda}_k = \psi_k \mathbf{1}_T$ for some $\psi_k \in \mathcal{R}$. Given the other $(q - 1)$ latent vectors, assumptions (6) and (7) imply that parameter ψ_k has a Dirichlet process conditional prior. The base distribution of the Dirichlet process is a mixture of a continuous distribution, $G_0 = N(\mu_G, \tau_G^2)$, and the univariate atoms located at the “known” elements of the other $(q - 1)$ latent vectors. The sufficient statistic for ψ_k is

$$\begin{aligned} \bar{y}_k &= \frac{1}{nm_k} \sum_{j=1}^p \sum_{i=1}^n (z_{ij} - \xi_i - \chi_j) \mathcal{I}(c_j = k) \\ &\sim N\left(\psi_k, \frac{\sigma^2}{nm_k}\right) \quad \text{for cluster } k \notin \mathcal{D}. \end{aligned}$$

Since the Dirichlet process conditional prior is conjugate to this normal likelihood, parameter ψ_k could be updated by Gibbs sampling (Escobar 1994, MacEachern 1994, Escobar & West 1995).

Differential clusters For these clusters, some of the T elements of latent vector $\boldsymbol{\lambda}_k = (\lambda_{1k}, \dots, \lambda_{Tk})'$ could be tied, but at least two elements must be unequal. Denote these restrictions on $\boldsymbol{\lambda}_k$ by \mathcal{A} . For a treatment t , let the remaining $(T - 1)$ elements of vector $\boldsymbol{\lambda}_k$ be denoted by $\boldsymbol{\lambda}_{-tk}$.

Imagine updating element λ_{tk} assuming that $\boldsymbol{\lambda}_{-tk}$ and the remaining $(q - 1)$ latent vectors are known. Vector $\boldsymbol{\lambda}_{-tk}$ and restriction \mathcal{A} imply a possibly restricted support,

\mathcal{A}_t , for parameter λ_{tk} . Observe that the support is unrestricted, i.e., $\mathcal{A}_t = \mathcal{R}$, if at least two elements of $\boldsymbol{\lambda}_{-tk}$ differ. Similarly to non-differential clusters, it can be shown that element λ_{tk} follows a Dirichlet process conditional prior restricted to the support \mathcal{A}_t , and that the base distribution is a mixture of a normal distribution and univariate atoms. The sufficient statistic for latent vector element λ_{tk} is

$$\begin{aligned} \bar{y}_{tk} &= \frac{1}{n_t m_k} \sum_{j=1}^p \sum_{i:t_i=t} (z_{ij} - \xi_i - \chi_j) \mathcal{I}(c_j = k) \\ &\sim N\left(\lambda_{tk}, \frac{\sigma^2}{n_t m_k}\right) \quad \text{for treatment } t = 1, \dots, T, \text{ and cluster } k \in \mathcal{D}, \end{aligned}$$

where n_t is the number of individuals associated with treatment t . The conjugate structure implies that parameter λ_{tk} could be generated from its full conditional by a rejection sampler on set \mathcal{A}_t coupled with standard Gibbs proposals for conjugate Dirichlet processes. In practice, the acceptance rates of the rejection sampler are very high for T as small as 3 or 4, and are nearly 100% for larger T . This is because the posterior probability of support set \mathcal{A}_t tends to 1 as T grows. An intuitive explanation for this asymptotic property is provided in Section 2.1.3 following the prior specification of discount parameter d_2 .

8 Additional details about Block 1 MCMC updates

In the first block of MCMC updates of Section 3.1, we sample the the set

$$\mathcal{C} = \{(g_j, s_j, v_j, \boldsymbol{\theta}_j) : j = 1, \dots, p\}.$$

We iteratively sample the 4-tuple, $(g_j, s_j, v_j, \boldsymbol{\theta}_j)$, for each probe j via Metropolis-Hastings updates. Specifically, for the j th probe, we propose group (i.e., restaurant) g_j , state (i.e., cuisine) s_j , PYP cluster (i.e., table) label v_j , and random effect (i.e., dish) $\boldsymbol{\theta}_j$, with the proposal distribution approximately equal to the joint posterior of $(g_j, s_j, v_j, \boldsymbol{\theta}_j)$ conditional on the data and all other parameters being equal to the current values. As explained in the paper, since the base measure of the Sticky PYP is discrete and not conjugate to the

likelihood, this makes the case of parameter v_j being assigned a new cluster label complicated. To deal with this situation, an auxiliary variable approach is used. Conditional on the current parameter values of the Dirichlet process prior for the latent vector elements, we generate a finite-dimensional approximation, G^* , to the Dirichlet process (Ishwaran & Zarepour 2002). Since the distribution G^* is discrete, it is characterized by a finite vector of probability masses, $\boldsymbol{\pi}$, and the corresponding values of probability mass points, \mathbf{u} . Then, conditional on the auxiliary variables from G^* , we obtain the quantities needed for the conditional posterior of v_j being assigned a new cluster label in the Metropolis-Hastings algorithm.

More formally, consider probe $j \in \{1, \dots, p\}$. The proposal probabilities for (g_j, s_j, v_j) are as follows:

- For an existing PYP cluster indexed by $v \in \{1, \dots, q_{gs}^{(-j)}\}$,

$$\begin{aligned}
Q(g_j = g, s_j = s, v_j = v) &= P(g_j = g, s_j = s, v_j = v \mid \mathbf{z}_j, \mathbf{c}^{(-j)}, \boldsymbol{\phi}_{gsv}, s_{j-1}, \eta, \rho, \gamma, \boldsymbol{\xi}, \boldsymbol{\chi}, \sigma^2) \\
&\propto [\mathbf{z}_j \mid v, s, g, \boldsymbol{\phi}_{gsv}, \boldsymbol{\xi}, \boldsymbol{\chi}, \sigma^2] P(v_j = v \mid \mathbf{c}^{(-j)}, s, g) P(s_j = s \mid g, \gamma, \rho) P(g_j = g \mid s_{j-1}, \eta, \gamma, \rho) \\
&\propto \prod_{i=1}^n \varphi(z_{ij} \mid \phi_{t_i gsv} + \xi_i + \chi_j, \sigma^2) (m_{gsv}^{(-j)} - d_s) \mathcal{Q}_g(s) \mathcal{F}_j(g). \tag{16}
\end{aligned}$$

- For a new PYP cluster indexed by $v^* = q_{gs}^{(-j)} + 1$,

$$\begin{aligned}
Q(g_j = g, s_j = s, v_j = v^*) &= P(g_j = g, s_j = s, v_j = v^* \mid \mathbf{z}_j, \mathbf{c}^{(-j)}, \boldsymbol{\pi}, \mathbf{u}, s_{j-1}, \eta, \rho, \gamma, \boldsymbol{\xi}, \boldsymbol{\chi}, \sigma^2) \\
&\propto [\mathbf{z}_j \mid v^*, s, g, \boldsymbol{\pi}, \mathbf{u}, \boldsymbol{\xi}, \boldsymbol{\chi}, \sigma^2] P(v_j = v^* \mid \mathbf{c}^{(-j)}, s, g) P(s_j = s \mid g, \gamma, \rho) P(g_j = g \mid s_{j-1}, \eta, \gamma, \rho) \\
&\propto \begin{cases} \sum_{l=1}^L \pi_l \left\{ \prod_{i=1}^n \varphi(z_{ij} \mid u_l + \xi_i + \chi_j, \sigma^2) \right\} (\alpha_1 + d_1 q_{g1}^{(-j)}) \mathcal{Q}_g(1) \mathcal{F}_j(g), & \text{if } s = 1, \\ \left\{ \prod_{t=1}^T \sum_{l=1}^L \pi_l \prod_{i:t_i=t} \varphi(z_{ij} \mid u_l + \xi_i + \chi_j, \sigma^2) - \sum_{l=1}^L \pi_l^T \prod_{i=1}^n \varphi(z_{ij} \mid u_l + \xi_i, \sigma^2) \right\} \\ \quad \times (\alpha_2 + d_2 q_{g2}^{(-j)}) \mathcal{Q}_g(2) \mathcal{F}_j(g), & \text{if } s = 2. \end{cases} \tag{17}
\end{aligned}$$

In expressions (16) and (17), when $j < p$, superscript $(-j)$ for a variable indicates that the calculation excludes the j th and $(j+1)$ th cluster allocation variables. Specifically,

$q_{gs}^{(-j)}$ denotes the number of PYP clusters for group g and state s ; $\mathbf{c}^{(-j)}$ denotes the vector of cluster allocations; $m_{gsv}^{(-j)}$ denotes the cluster membership count for cluster v in the PYP with group g and state s ; $\mathcal{Q}_g(s)$ and $\mathcal{F}_j(g)$ are defined in the paper; $\varphi(\cdot | \mu, \sigma^2)$ is the density of the normal distribution with mean μ and variance σ^2 ; L is the number of distinct mass points in G^* ; u_l denotes the value of distinct mass points in G^* and π_l is the corresponding probability mass. Before calculating the proposal, latent vectors of emptied clusters are removed and cluster labels rearranged so that the largest label is $q_{gs}^{(-j)}$.

The case $v^* = (q_{gs}^{(-j)} + 1)$ corresponds to the case of v_j opening a new cluster. If $v_j = (q_{gs}^{(-j)} + 1)$ has been proposed, then a new random effect of length T is sampled from the posterior distribution based on the n -dimensional observation vector \mathbf{z}_j and the prior G^* characterized by the auxiliary variables, subject to the constraints imposed on the random effects of the differential state s_j .

The Metropolis-Hastings acceptance ratio is computed to decide whether the proposed g_j , s_j and v_j values are accepted. For $j = p$, our proposal density is exactly the desired conditional posterior, so we always accept the move. For $j < p$, since our proposal density is part of the desired conditional posterior for (g_j, s_j, v_j) , this part cancels out in the acceptance ratio. Therefore, the acceptance ratio only relates to the transition from (g_j, s_j, v_j) to $(g_{j+1}, s_{j+1}, v_{j+1})$, which is

$$r_j = \frac{p\left(g_{j+1}, s_{j+1}, \tilde{v}_{j+1}, | g_j^*, s_j^*, v_j^*, \phi_{g_{j+1}s_{j+1}\tilde{v}_{j+1}}^*, \mathbf{z}_{j+1}, \mathbf{c}^-, \eta, \xi, \chi, \sigma\right)}{p\left(g_{j+1}, s_{j+1}, v_{j+1} | g_j^0, s_j^0, v_j^0, \phi_{g_{j+1}s_{j+1}v_{j+1}}, \mathbf{z}_{j+1}, \mathbf{c}^-, \eta, \xi, \chi, \sigma\right)} \quad (18)$$

where g_j^* , s_j^* and v_j^* represent the proposed values; g_j^0 , s_j^0 and v_j^0 are the old values; \tilde{v}_{j+1} denotes v_{j+1} under the proposed variable values (due to possible PYP cluster label change or elimination). Specifically, $\tilde{v}_{j+1} = (q_{g_{j+1}s_{j+1}}^* + 1)$ if it belongs to no existing cluster, where $q_{g_{j+1}s_{j+1}}^*$ is the number of clusters under the proposed variable values and $\phi_{g_{j+1}s_{j+1}\tilde{v}_{j+1}}^*$ is the random effect under the proposed variable values. Both the nominator and the denominator in (18) can be calculated using (16) and (17), and by transposing j to $(j + 1)$.

9 Generalized form of the Sticky PYP

A Sticky PYP is defined by the following general properties:

Property 1: Set \mathcal{G} comprises a countable number of generative *groups*. Each group $g \in \mathcal{G}$ contains a countable number of group-specific regular PYPs. The PYPs are identified by a combination of the group label g and an integer-valued *state*, $s \in \mathcal{S}$. In other words, the PYPs have bivariate labels, $(g, s) \in \mathcal{G} \times \mathcal{S}$.

Property 2: For every $(g, s) \in \mathcal{G} \times \mathcal{S}$, let the corresponding PYP be $\mathcal{W}_{gs}(d_s, \alpha_s, W_s)$, of which the T -variate base distribution W_s , discount parameter $d_s \in [0, 1)$, and mass parameter $\alpha_s > 0$ depend on the state s . If set \mathcal{S} contains multiple states, assume that the base distributions $\{W_s : s \in \mathcal{S}\}$ are such that two PYPs associated with unequal states almost surely have non-intersecting sets of atoms.

Let distribution \mathcal{P}_{gs} be an independent realizations of the corresponding PYP:

$$\mathcal{P}_{gs} \mid d_s, \alpha_s, W_s \stackrel{indep}{\sim} \mathcal{W}_{gs}(d_s, \alpha_s, W_s), \quad (g, s) \in \mathcal{G} \times \mathcal{S}.$$

Consequently, for each s , the distributions $\{\mathcal{P}_{gs} : g \in \mathcal{G}\}$ share the same atoms as base distribution W_s ; however, the probabilities associated with the atoms depend on the group-state combination.

Property 3: For probe $j = 1, \dots, p$, the label of the PYP generating the random effect θ_j is denoted by $(g_j, s_j) \in \mathcal{G} \times \mathcal{S}$, and $\theta_j \mid \mathcal{P}_{g_j s_j} \stackrel{indep}{\sim} \mathcal{P}_{g_j s_j}$.

Property 4: Given the group g_j of the j^{th} probe, the state has the distribution:

$$s_j \mid g_j \sim \mathcal{Q}_{g_j}$$

where, for every $g \in \mathcal{G}$, \mathcal{Q}_g denotes a group-specific probability mass function on the set \mathcal{S} ; thus, $\sum_{s \in \mathcal{S}} \mathcal{Q}_g(s) = 1$.

Property 5: (*Markov property*) For the first probe, group g_1 follows a categorical distribution, \mathcal{F}_1 , on the set \mathcal{G} . For the subsequent probes $j > 1$, given the variables associated with the preceding probes, the mass function of group variable g_j generally depends on probe index j , random vector $\boldsymbol{\theta}_{j-1}$, and inter-probe distance e_{j-1} :

$$g_j \sim \mathcal{F}_{j\boldsymbol{\theta}_{j-1}e_{j-1}}$$

where, for every $\boldsymbol{\theta} \in \mathcal{R}^T$ and $e > 0$, $\mathcal{F}_{j\boldsymbol{\theta}e}$ denotes a probability mass function on the set \mathcal{G} , so that $\sum_{g \in \mathcal{G}} \mathcal{F}_{j\boldsymbol{\theta}e}(g) = 1$.

Some popular examples are presented in Table 2 of Supplementary Material. As suggested by the form of distribution $\mathcal{F}_{j\boldsymbol{\theta}e}$ in the table, rows 1–5 of Table 2 display zero order Sticky PYPs, e.g., hierarchical Pitman-Yor processes (HPYP) (Teh et al. 2006, Camerlenghi et al. 2019). Rows 6 and 7 are first order Sticky PYPs involving multiple groups and single states. The mass functions $\mathcal{F}_{j\boldsymbol{\theta}e}$ do not depend on inter-probe distance e in the examples.

For a detailed discussion of a specific mixture model, consider the hierarchical Dirichlet process (HDP) of Teh et al. (2006), in which p objects are organized into K groups with known group memberships g_1, \dots, g_p . Let global measure W_∞ be a Dirichlet process realization, and therefore, a countably infinite distribution in \mathcal{R}^T . The random effects $\boldsymbol{\theta}_1, \dots, \boldsymbol{\theta}_p$ are distributed as:

$$\begin{aligned} \boldsymbol{\theta}_j &| G_{g_j} \stackrel{indep}{\sim} G_{g_j}, \quad j = 1, \dots, p, \\ G_g &| \alpha, W_\infty \stackrel{i.i.d.}{\sim} \text{DP}(\alpha, W_\infty), \quad g = 1, \dots, K. \end{aligned} \tag{19}$$

As summarized in the fourth row of Table 2, the model can be recast as a generalized Sticky PYP as follows:

Property 1: The set of group labels, $\mathcal{G} = \{1, \dots, K\}$. An HDP is a single-state model with state set $\mathcal{S} = \{1\}$, i.e., $s_j = 1$ for all p objects. To simplify the notation, we henceforth drop the subscript s .

Property 2: For group $g = 1, \dots, K$, the associated PYP is $\mathcal{W}_g(0, \alpha, W_\infty) = \text{DP}(\alpha, W_\infty)$.

Property 3: Since distribution \mathcal{P}_g in the generalized Sticky PYP formulation is a random realization of $\mathcal{W}_{\infty g}(0, \alpha, W_\infty) = \text{DP}(\alpha, W_\infty)$, we identify $\mathcal{P}_g = G_g$ in expression (19).

Property 4: An HDP is a single-state model; therefore, trivially, $\mathcal{Q}_g = 1_{\{1\}}$.

Property 5: Group variables g_1, \dots, g_p are known. Hence, $\mathcal{F}_1 = 1_{\{g_1\}}$ and $\mathcal{F}_{j\theta,e} = 1_{\{g_j\}}$, $j = 2, \dots, p$.

The 2R2CF used in differential methylation is a Sticky PYP with two groups and two states. A key characteristic distinguishing it from the other first order models, and indeed, all the models listed in Table 2, is that the 2R2CF makes a probabilistic, rather than deterministic, assumption for group variable g_j that varies with the inter-probe distances. As noted in Section 2.1, the 2R2CF behaves similarly to two-state hidden Markov models for very small inter-probe distances and similarly to finite mixture models for relatively large distances. For differential analysis, this offers a key advantage in datasets with widely varying inter-probe distances by allowing the differential and non-differential probes to have different cluster allocation patterns depending on the differential statuses and distances of adjacent probes. These interpretable features of the 2R2CF process are facilitated by the two-group, two-state construct.

Model	\mathcal{G}	$\mathcal{W}_{gs}(d_s, \alpha_s, W_s)$	$\mathcal{F}_{j\theta e}$
Finite mixture	$\{1\}$	$\mathcal{W}(0, \alpha, W_K)$,	$1_{\{1\}}$
Dirichlet process	$\{1\}$	$\mathcal{W}(0, \alpha, W)$	$1_{\{1\}}$
PYP	$\{1\}$	$\mathcal{W}(d, \alpha, W)$	$1_{\{1\}}$
HDP	\mathcal{N}_K	$\mathcal{W}_g(0, \alpha, W_\infty)$	$1_{\{g_j\}}$; known $g_j \in \mathcal{G}$
HPYP	\mathcal{N}_K	$\mathcal{W}_g(d, \alpha, W_\infty)$	$1_{\{g_j\}}$; known $g_j \in \mathcal{G}$
Finite HMM	\mathcal{N}_K	$\mathcal{W}_g(0, \alpha, W_K)$	Point mass at $\sum_{v=1}^K v \cdot \mathcal{I}(\theta = \phi_v)$
HDP-HMM	\mathcal{N}	$\mathcal{W}_g(0, \alpha, W_\infty)$	Point mass at $\sum_{v=1}^\infty v \cdot \mathcal{I}(\theta = \phi_v)$

Table 2: Examples of Sticky PYPs. The examples listed here correspond to a singleton state set, $\mathcal{S} = \{1\}$, and degenerate distribution, $\mathcal{Q}_g = 1_{\{1\}}$. Set \mathcal{N} represents the natural numbers, $\mathcal{N}_K = \{1, \dots, K\}$ for some $K > 1$, $d \in [0, 1)$, and W is an arbitrary distribution in \mathcal{R}^T . Distribution W_K is finite with T -variate atoms $\{\phi_v\}_{v=1}^K$. Distribution W_∞ is countably infinite with T -variate atoms $\{\phi_v\}_{v=1}^\infty$. In an HDP or HDP-HMM, W_∞ represents a Dirichlet process realization. For an HPYP, W_∞ represents a PYP realization. Refer to Section 9 for the notation and further discussion.

		Low noise		High noise	
		High correlation	No correlation	High correlation	No correlation
AUC	BayesDiff	0.995	0.970	0.944	0.830
	ANOVA	0.964	0.949	0.888	0.864
	Kruskal-Wallis	0.958	0.944	0.878	0.854
	COHCAP	0.955	0.941	0.861	0.841
	Methylkit	0.955	0.942	0.869	0.848
	BiSeq	0.949	0.933	0.867	0.845
	RADMeth	0.959	0.944	0.876	0.852
AUC ₂₀	BayesDiff	0.988	0.926	0.884	0.636
	ANOVA	0.891	0.851	0.684	0.628
	Kruskal-Wallis	0.876	0.833	0.657	0.597
	COHCAP	0.856	0.820	0.602	0.556
	Methylkit	0.858	0.819	0.633	0.579
	BiSeq	0.822	0.781	0.607	0.559
	RADMeth	0.871	0.833	0.639	0.588
AUC ₁₀	BayesDiff	0.985	0.901	0.857	0.565
	ANOVA	0.849	0.804	0.586	0.529
	Kruskal-Wallis	0.827	0.773	0.551	0.493
	COHCAP	0.797	0.751	0.492	0.433
	Methylkit	0.794	0.744	0.523	0.458
	BiSeq	0.726	0.673	0.482	0.424
	RADMeth	0.817	0.775	0.531	0.471

Table 3: Areas under ROC curves for the different methods (rows) under the four simulation scenarios (columns). See the text in the paper for further discussion.

BayesDiff					
Gene	DM Proportion	Largest Difference	Gene	DM Proportion	Largest Difference
EDNRB	1.00	STAD↑ LIHC↓	SLITRK1	0.96	STAD↑ LIHC↓
PCLO	1.00	PAAD↑ LIHC↓	FLRT2	0.96	STAD↑ LIHC↓
PREX2	1.00	STAD↑ LIHC↓	KCNA1	0.96	STAD↑ LIHC↓
SLIT2	1.00	STAD↑ LIHC↓	TRPA1	0.96	STAD↑ LIHC↓
SLITRK2	1.00	STAD↑ LIHC↓	ADCY8	0.96	STAD↑ LIHC↓
SORCS3	1.00	STAD↑ LIHC↓	CTNNA2	0.95	PAAD↑ LIHC↓
SPHKAP	1.00	ESCA↑ LIHC↓	GRIA2	0.95	STAD↑ LIHC↓
SPTA1	1.00	PAAD↑ LIHC↓	ADGRL3	0.94	PAAD↑ LIHC↓
UNC13C	1.00	PAAD↑ LIHC↓	LRRC7	0.94	STAD↑ LIHC↓
XIRP2	1.00	PAAD↑ LIHC↓	ERBB4	0.93	PAAD↑ LIHC↓
ZNF804B	1.00	STAD↑ LIHC↓	PCDH10	0.93	STAD↑ LIHC↓
TSHZ3	0.97	STAD↑ LIHC↓	SOX11	0.93	STAD↑ LIHC↓
MYO3A	0.97	STAD↑ LIHC↓	NLGN4X	0.93	PAAD↑ LIHC↓
ABCC9	0.97	ESCA↑ LIHC↓	NBEA	0.93	PAAD↑ LIHC↓
EPB41L3	0.97	STAD↑ LIHC↓	CNTN1	0.92	STAD↑ LIHC↓
FBN2	0.97	STAD↑ LIHC↓	GRM5	0.92	PAAD↑ LIHC↓
PCDH17	0.96	STAD↑ LIHC↓	PTPRZ1	0.91	STAD↑ PAAD↓
CDH8	0.96	STAD↑ LIHC↓	EPHA5	0.91	STAD↑ LIHC↓

Table 4: For **BayesDiff**, genes with the overall proportion of differentially methylated CpG sites exceeding 0.9. The “Largest Difference” column displays which pair-wise difference between the four cancer types is the largest, with the symbol “↑ (↓)” indicating higher (lower) methylation level for one cancer type relative to the other.

BayesDiff			
Gene	Number of probes	Gene	Number of probes
ABCC9	36	NLGN4X	28
ADCY8	24	PCDH10	30
ADGRL3	35	PCDH17	27
CDH8	26	PCLO	20
CNTN1	25	PREX2	21
CTNNA2	85	PTPRZ1	23
EDNRB	56	SLIT2	29
EPB41L3	34	SLITRK1	26
EPHA5	22	SLITRK2	28
ERBB4	30	SORCS3	39
FBN2	30	SOX11	44
FLRT2	51	SPHKAP	17
GRIA2	20	SPTA1	16
GRM5	25	TRPA1	25
KCNA1	25	TSHZ3	39
LRRC7	34	UNC13C	11
MYO3A	38	XIRP2	19
NBEA	55	ZNF804B	21

Table 5: Number of included CpG sites for the top methylated genes listed in Table 4 for BayesDiff.

BayesDiff and ANOVA				
Gene	DM Proportion	Largest Difference	DM Proportion	Largest Difference
	BayesDiff	BayesDiff	ANOVA	ANOVA
PCLO	1.00	PAAD↑ LIHC↓	1.00	PAAD↑ LIHC↓
UNC13C	1.00	PAAD↑ LIHC↓	1.00	PAAD↑ ESCA↓
XIRP2	1.00	PAAD↑ LIHC↓	1.00	PAAD↑ STAD↓
ZNF804B	1.00	STAD↑ LIHC↓	1.00	ESCA↑ PAAD↓
FBN2	0.97	STAD↑ LIHC↓	0.93	PAAD↑ STAD↓
FLRT2	0.96	STAD↑ LIHC↓	0.92	STAD↑ PAAD↓
ERBB4	0.93	PAAD↑ LIHC↓	0.93	STAD↑ PAAD↓
PTPRZ1	0.91	STAD↑ PAAD↓	0.91	PAAD↑ LIHC↓

Table 6: For both **BayesDiff** and **ANOVA** methods, the common set of genes detected with the overall proportion of differentially methylated CpG sites exceeding 0.9. For each method, the “Largest Difference” column displays which pair-wise difference between the four cancer types is the largest, with the symbol “↑ (↓)” indicating higher (lower) methylation level for one cancer type relative to the other.

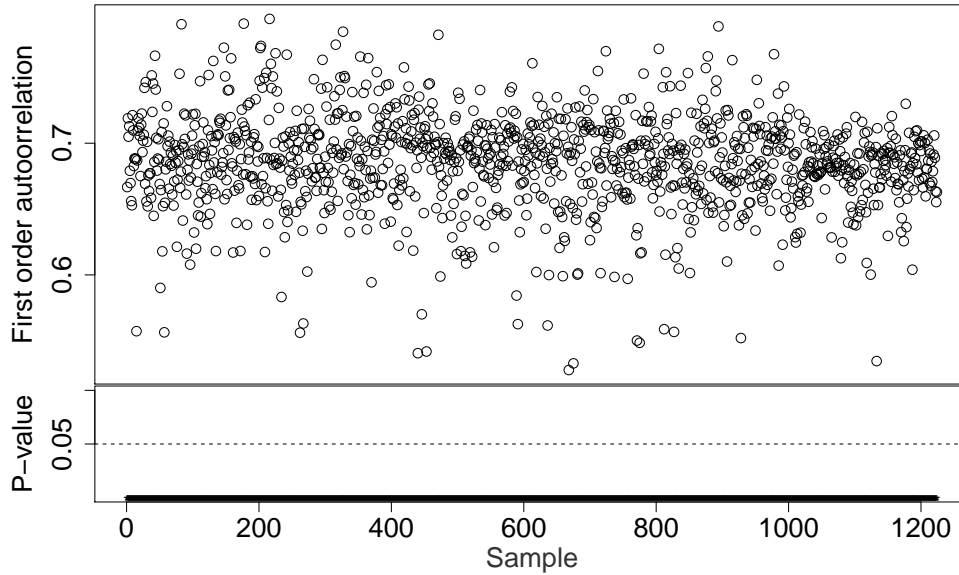
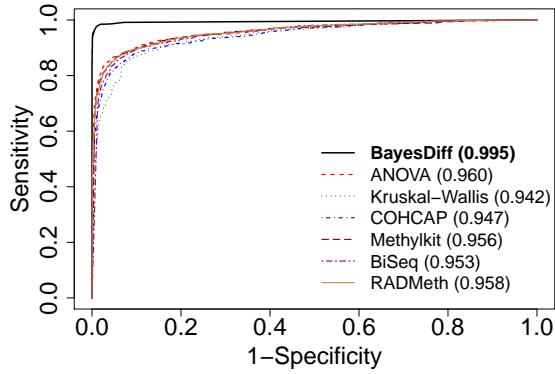


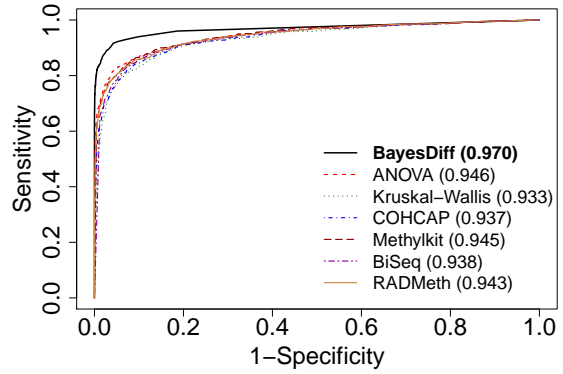
Figure 6: Exploratory analysis of DNA methylation profiles of upper GI cancer samples from TCGA. See the text in the paper for further explanation.

References

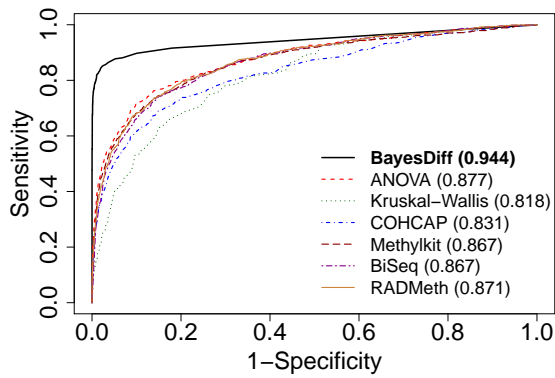
- Akalin, A., Kormaksson, M., Li, S., Garrett-Bakelman, F. E., Figueroa, M. E., Melnick, A. & Mason, C. E. (2012), ‘methylkit: a comprehensive r package for the analysis of genome-wide dna methylation profiles’, *Genome Biology* **13**(10), R87. [5](#), [27](#)
- Bae, H., Kim, B., Lee, H., Lee, S., Kang, H.-S. & Kim, S. J. (2017), ‘Epigenetically regulated fibronectin leucine rich transmembrane protein 2 (flrt2) shows tumor suppressor activity in breast cancer cells’, *Scientific Reports* **7**(1), 272. [32](#)
- Baker, T. A., Bell, S. P., Gann, A., Levine, M., Losick, R. & Inglis, C. (2008), *Molecular biology of the gene*, San Francisco, CA, USA:: Pearson/Benjamin Cummings. [7](#)
- Basu, S. & Chib, S. (2003), ‘Marginal likelihood and bayes factors for dirichlet process mixture models’, *Journal of the American Statistical Association* **98**(461), 224–235. [25](#)



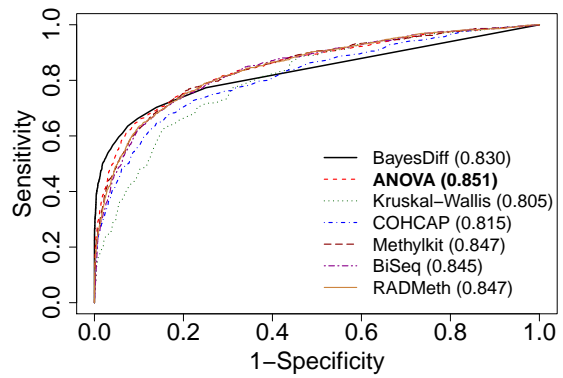
(a) Low noise, high correlation



(b) Low noise, no correlation

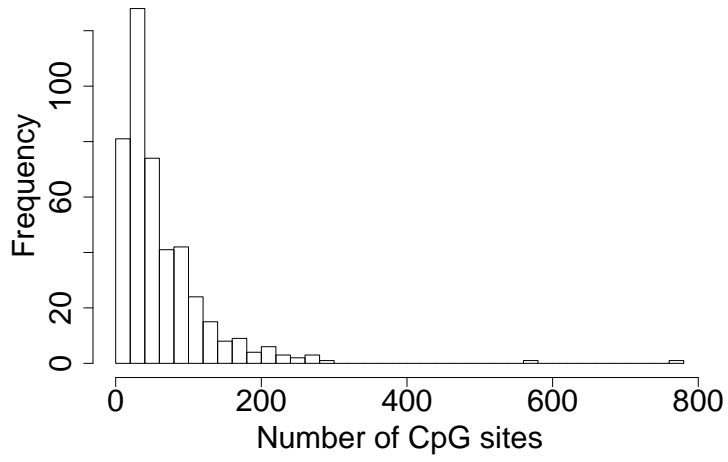


(c) High noise, high correlation

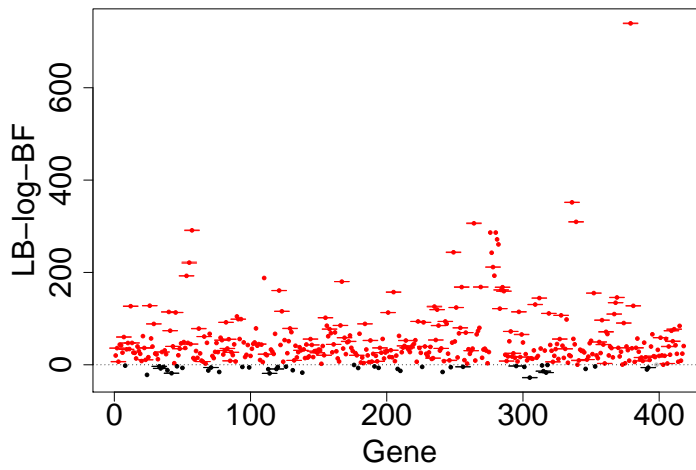


(d) High noise, no correlation

Figure 7: ROC curves, averaged over 20 simulated datasets, for the seven methods and the four simulation scenarios. The numbers in parentheses represent AUCs.

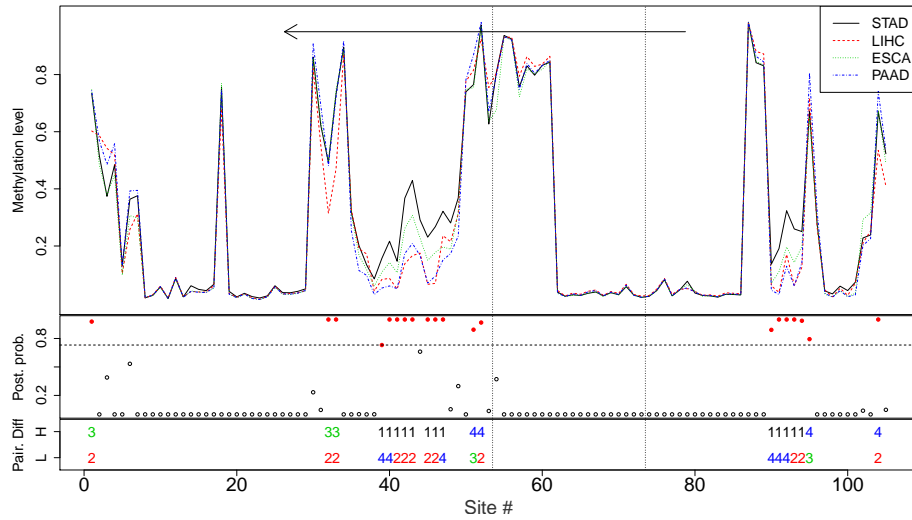


(a) Histogram of the number of gene-specific CpG sites

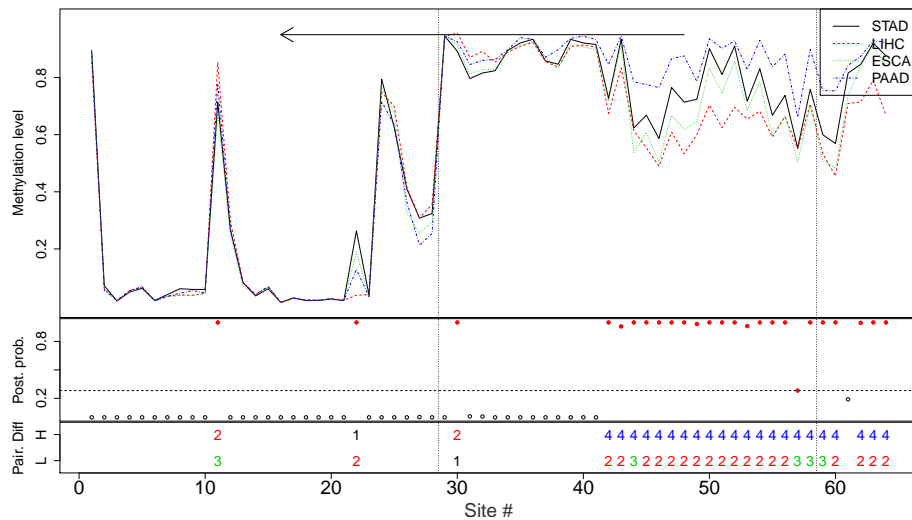


(b) 95% credible intervals for lower bounds of log-Bayes factors of first order versus zero-order models. The intervals whose lower limits are positive are marked in red.

Figure 8: Data analysis plots. See the Section 5 text for further explanation.

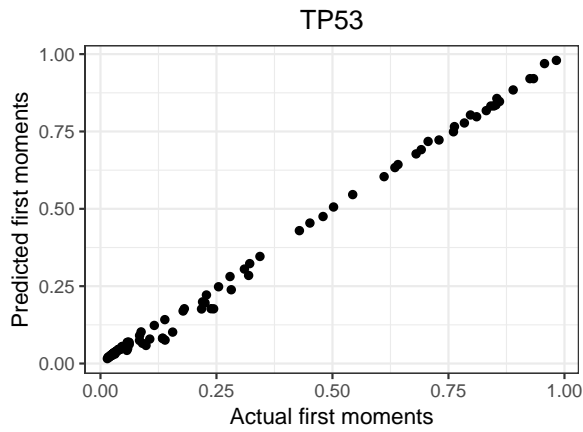


(a) Gene TP53

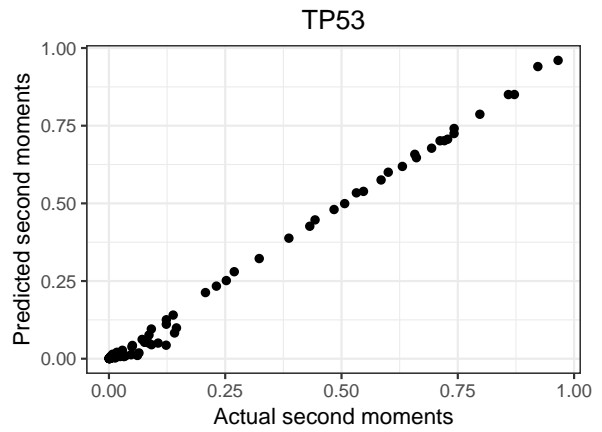


(b) Gene TTN

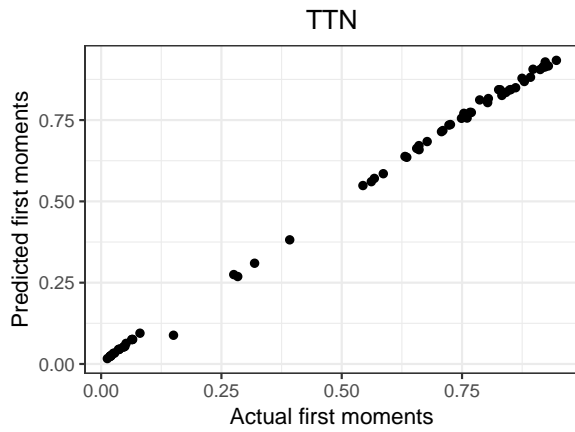
Figure 9: Detailed differential methylation results for the top 2 mutated genes. For each gene, the upper panel shows the mean methylation levels. The middle panel shows the posterior probabilities of each CpG site being differentially methylated, with solid points representing differential methylation and dashed line denoting the corresponding cutoff value. The lower panel indicates the largest pairwise difference between the 4 cancer types. Symbols 1–4 in the lower panel represent GI₅₃₈ cancer types STAD, LIHC, ESCA and PAAD, respectively. The vertical dotted lines represent the gene boundaries. The arrow at the top indicates the transcription direction.



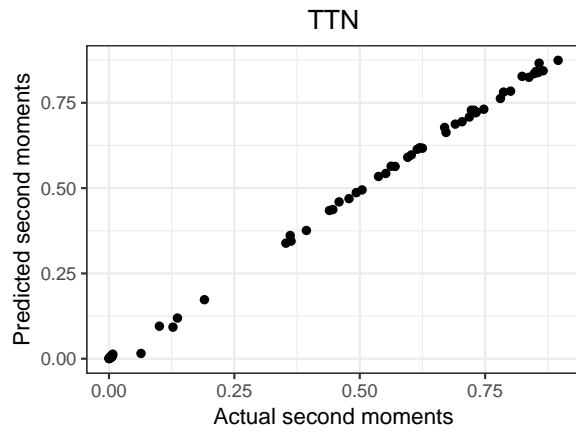
(a) First moments for gene TP53



(b) Second moments for gene TP53



(c) First moments for gene TTN



(d) Second moments for gene TTN

Figure 10: Comparison of predicted and actual sample moments for the 2 top mutated genes.

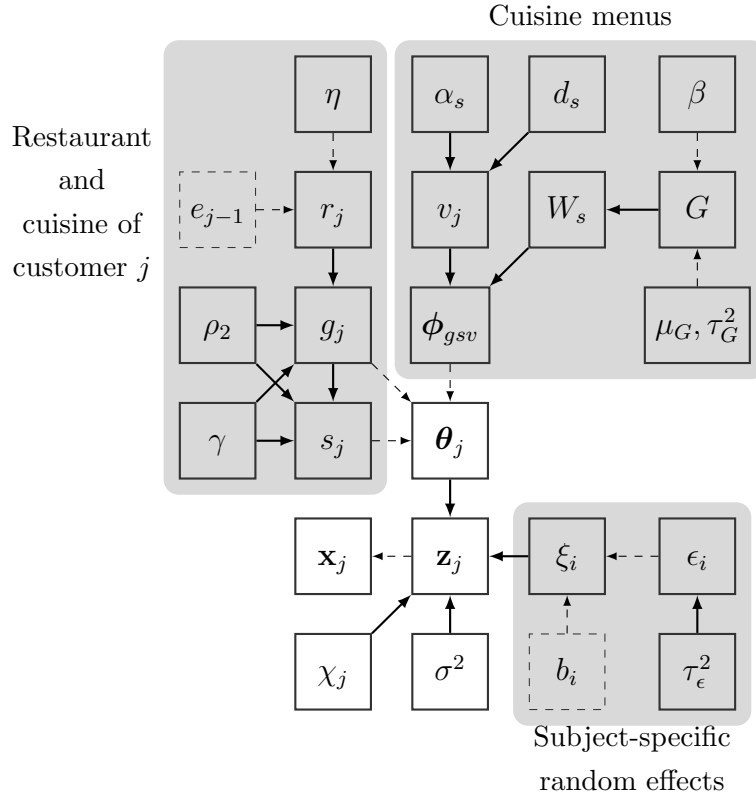


Figure 11: Directed acyclic graph of the BayesDiff model showing the relationships between the model parameters. Solid rectangles represent the data and model parameters. Dashed rectangles represent predetermined constants. Solid arrows represent stochastic relationships, and dashed arrows represent deterministic relationships.

ANOVA, not BayesDiff					
Gene	DM Proportion	Largest Difference	Gene	DM Proportion	Largest Difference
LRP12	1.00	LIHC↑ STAD↓	EPHA6	0.95	STAD↑ PAAD↓
PTPRM	1.00	STAD↑ LIHC↓	RELN	0.95	STAD↑ LIHC↓
SALL1	0.96	STAD↑ LIHC↓	COL6A6	0.94	STAD↑ LIHC↓
TIAM1	0.96	LIHC↑ PAAD↓	MUC16	0.94	PAAD↑ LIHC↓
MXRA5	0.96	LIHC↑ PAAD↓	HCN1	0.91	PAAD↑ ESCA↓
ZFHX4	0.96	LIHC↑ STAD↓	RIMS2	0.91	STAD↑ LIHC↓

Table 7: For **only ANOVA but not BayesDiff**, genes detected with the overall proportion of differentially methylated CpG sites exceeding 0.9. The “Largest Difference” column displays which pair-wise difference between the four cancer types is the largest, with the symbol “↑ (↓)” indicating higher (lower) methylation level for one cancer type relative to the other.

Benjamini, Y. & Hochberg, Y. (1995), ‘Controlling the false discovery rate: a practical and powerful approach to multiple testing’, *Journal of the Royal Statistical Society: Series B (Methodological)* pp. 289–300. [27](#)

Blei, D. M. & Jordan, M. I. (2005), ‘Variational inference for dirichlet process mixtures’, *Bayesian Analysis* **1**, 1–23. [35](#)

Camerlenghi, F., Lijoi, A., Orbanz, P. & Prünster, I. (2019), ‘Distribution theory for hierarchical processes’, *The Annals of Statistics* **47**(1), 67 – 92. [35](#), [43](#)

Chib, S. (1995), ‘Marginal likelihood from the gibbs output’, *Journal of the American Statistical Association* **90**(432), 1313–1321. [25](#)

Chib, S. & Winkelmann, R. (2001), ‘Markov chain monte carlo analysis of correlated count data’, *Journal of Business & Economic Statistics* **19**(4), 428–435. [34](#)

BayesDiff, not ANOVA					
Gene	DM Proportion	Largest Difference	Gene	DM Proportion	Largest Difference
EDNRB	1.00	STAD↑ LIHC↓	KCNA1	0.96	STAD↑ LIHC↓
PREX2	1.00	STAD↑ LIHC↓	TRPA1	0.96	STAD↑ LIHC↓
SLIT2	1.00	STAD↑ LIHC↓	ADCY8	0.96	STAD↑ LIHC↓
SLITRK2	1.00	STAD↑ LIHC↓	CTNNA2	0.95	PAAD↑ LIHC↓
SORCS3	1.00	STAD↑ LIHC↓	GRIA2	0.95	STAD↑ LIHC↓
SPHKAP	1.00	ESCA↑ LIHC↓	ADGRL3	0.94	PAAD↑ LIHC↓
SPTA1	1.00	PAAD↑ LIHC↓	LRRC7	0.94	STAD↑ LIHC↓
TSHZ3	0.97	STAD↑ LIHC↓	PCDH10	0.93	STAD↑ LIHC↓
MYO3A	0.97	STAD↑ LIHC↓	SOX11	0.93	STAD↑ LIHC↓
ABCC9	0.97	ESCA↑ LIHC↓	NLGN4X	0.93	PAAD↑ LIHC↓
EPB41L3	0.97	STAD↑ LIHC↓	NBEA	0.93	PAAD↑ LIHC↓
PCDH17	0.96	STAD↑ LIHC↓	CNTN1	0.92	STAD↑ LIHC↓
CDH8	0.96	STAD↑ LIHC↓	GRM5	0.92	PAAD↑ LIHC↓
SLITRK1	0.96	STAD↑ LIHC↓	EPHA5	0.91	STAD↑ LIHC↓

Table 8: For **only BayesDiff but not ANOVA**, genes detected with overall proportion of differentially methylated CpG sites exceeding 0.9. The “Largest Difference” column displays which pair-wise difference between the four cancer types is the largest, with the symbol “↑ (↓)” indicating higher (lower) methylation level for one cancer type relative to the other.

- De Blasi, P., Favaro, S., Lijoi, A., Mena, R. H., Prünster, I. & Ruggiero, M. (2013), ‘Are gibbs-type priors the most natural generalization of the dirichlet process?’, *IEEE transactions on pattern analysis and machine intelligence* **37**(2), 212–229. [9](#)
- Dolzhenko, E. & Smith, A. D. (2014), ‘Using beta-binomial regression for high-precision differential methylation analysis in multifactor whole-genome bisulfite sequencing experiments’, *BMC bioinformatics* **15**(1), 215. [5](#), [27](#)
- Du, P., Zhang, X., Huang, C.-C., Jafari, N., Kibbe, W. A., Hou, L. & Lin, S. M. (2010), ‘Comparison of beta-value and m-value methods for quantifying methylation levels by microarray analysis’, *BMC bioinformatics* **11**, 1–9. [7](#)
- Dunson, D. B., Herring, A. H. & Engel, S. M. (2008), ‘Bayesian selection and clustering of polymorphisms in functionally-related genes’, *Journal of the American Statistical Association* **103**, 534–546. [8](#)
- Dunson, D. B. & Park, J.-H. (2008), ‘Kernel stick-breaking processes’, *Biometrika* **95**, 307–323. [8](#)
- Durbin, B., Hardin, J., Hawkins, D. & Rocke, D. (2002), ‘A variance-stabilizing transformation for gene-expression microarray data’, *Bioinformatics* **18**, S105—S110. [34](#)
- Eckhardt, F., Lewin, J., Cortese, R., Rakyan, V. K., Attwood, J., Burger, M., Burton, J., Cox, T. V., Davies, R., Down, T. A. et al. (2006), ‘Dna methylation profiling of human chromosomes 6, 20 and 22’, *Nature Genetics* **38**(12), 1378. [4](#)
- Escobar, M. D. (1994), ‘Estimating normal means with a dirichlet process prior’, *Journal of the American Statistical Association* **89**(425), 268–277. [38](#)
- Escobar, M. D. & West, M. (1995), ‘Bayesian density estimation and inference using mixtures’, *Journal of the American statistical association* **90**(430), 577–588. [38](#)
- Feinberg, A. P. & Tycko, B. (2004), ‘The history of cancer epigenetics’, *Nature reviews. Cancer* **4**(2), 143. [3](#)

- Feng, H., Conneely, K. N. & Wu, H. (2014), ‘A bayesian hierarchical model to detect differentially methylated loci from single nucleotide resolution sequencing data’, *Nucleic Acids Research* **42**(8), e69–e69. [5](#)
- Ferguson, T. S. (1973*a*), ‘A bayesian analysis of some nonparametric problems’, *The Annals of Statistics* pp. 209–230. [8](#)
- Ferguson, T. S. (1973*b*), ‘A bayesian analysis of some nonparametric problems’, *Annals of Statistics* **1**, 209–223. [18](#)
- Fox, E., Sudderth, E., Jordan, M. & Willsky, A. (2011), ‘The sticky hdp-hmm: Bayesian nonparametric hidden markov models with persistent states’, *Annals of Applied Statistics* **5**, 1020–1056. [9](#)
- Frühwirth-Schnatter, S. (2006), *Finite Mixture and Markov Switching Models*, New York: Springer. [21](#)
- Gnedin, A. & Pitman, J. (2006), ‘Exchangeable gibbs partitions and stirling triangles’, *Journal of Mathematical Sciences* **138**, 5674–5685. [9](#)
- Grossman, R. L., Heath, A. P., Ferretti, V., Varmus, H. E., Lowy, D. R., Kibbe, W. A. & Staudt, L. M. (2016), ‘Toward a shared vision for cancer genomic data’, *New England Journal of Medicine* **375**(12), 1109–1112. [29](#)
- Guha, S. (2010), ‘Posterior simulation in countable mixture models for large datasets’, *Journal of the American Statistical Association* **105**(490), 775–786. [28](#)
- Guha, S. & Baladandayuthapani, V. (2016), ‘A nonparametric bayesian technique for high-dimensional regression’, *Electronic Journal of Statistics* **10**, 3374–3424. [8](#), [9](#), [20](#)
- Hansen, K. D., Langmead, B. & Irizarry, R. A. (2012), ‘Bsmooth: from whole genome bisulfite sequencing reads to differentially methylated regions’, *Genome Biology* **13**(10), R83. [4](#), [5](#), [9](#)

- Hebestreit, K., Dugas, M. & Klein, H.-U. (2013), ‘Detection of significantly differentially methylated regions in targeted bisulfite sequencing data’, *Bioinformatics* **29**(13), 1647–1653. [5](#), [9](#), [27](#)
- Irizarry, R. A., Ladd-Acosta, C., Carvalho, B., Wu, H., Brandenburg, S. A., Jeddloh, J. A., Wen, B. & Feinberg, A. P. (2008), ‘Comprehensive high-throughput arrays for relative methylation (charm)’, *Genome Research* **18**(5), 780–790. [4](#)
- Irizarry, R. A., Ladd-Acosta, C., Wen, B., Wu, Z., Montano, C., Onyango, P., Cui, H., Gabo, K., Rongione, M., Webster, M. et al. (2009), ‘Genome-wide methylation analysis of human colon cancer reveals similar hypo- and hypermethylation at conserved tissue-specific CpG island shores’, *Nature Genetics* **41**(2), 178. [3](#), [30](#)
- Ishwaran, H. & James, L. F. (2003), ‘Generalized weighted Chinese restaurant processes for species sampling mixture models’, *Statistica Sinica* **13**, 1211–1235. [12](#)
- Ishwaran, H. & Zarepour, M. (2002), ‘Dirichlet prior sieves in finite normal mixtures’, *Statistica Sinica* **12**, 941–963. [37](#), [40](#)
- Jaffe, A. E., Murakami, P., Lee, H., Leek, J. T., Fallin, M. D., Feinberg, A. P. & Irizarry, R. A. (2012), ‘Bump hunting to identify differentially methylated regions in epigenetic epidemiology studies’, *International Journal of Epidemiology* **41**(1), 200–209. [5](#), [9](#)
- Kim, S., Tadesse, M. G. & Vannucci, M. (2006), ‘Variable selection in clustering via Dirichlet process mixture models’, *Biometrika* **93**, 877–893. [8](#)
- Leek, J. T., Scharpf, R. B., Bravo, H. C., Simcha, D., Langmead, B., Johnson, W. E., Geman, D., Baggerly, K. & Irizarry, R. A. (2010), ‘Tackling the widespread and critical impact of batch effects in high-throughput data’, *Nature Reviews Genetics* **11**(10). [4](#)
- Li, D., Wang, X., Lin, L. & Dey, D. K. (2016), ‘Flexible link functions in nonparametric binary regression with Gaussian process priors’, *Biometrics* **72**(3), 707–719. [34](#)
- Lijoi, A., Mena, R. & Prünster, I. (2007a), ‘Bayesian nonparametric estimation of the probability of discovering new species’, *Biometrika* **94**, 769–786. [8](#)

- Lijoi, A., Mena, R. & Prünster, I. (2007*b*), ‘Controlling the reinforcement in bayesian non-parametric mixture models’, *Journal of the Royal Statistical Society: Series B (Statistical Methodology)* **69**, 715–740. [10](#)
- Lijoi, A. & Prünster, I. (2010), *Models beyond the Dirichlet process*, Cambridge Series in Statistical and Probabilistic Mathematics, pp. 80–136. [12](#), [18](#)
- MacEachern, S. N. (1994), ‘Estimating normal means with a conjugate style dirichlet process prior’, *Communications in Statistics-Simulation and Computation* **23**(3), 727–741. [38](#)
- Medvedovic, M., Yeung, K. Y. & Bumgarner, R. E. (2004), ‘Bayesian mixture model based clustering of replicated microarray data’, *Bioinformatics* **20**, 1222–1232. [8](#)
- Müller, P. & Mitra, R. (2013), ‘Bayesian nonparametric inference—why and how’, *Bayesian Analysis (Online)* **8**(2). [8](#)
- Murphy, S. J., Hart, S. N., Lima, J. F., Kipp, B. R., Klebig, M., Winters, J. L., Szabo, C., Zhang, L., Eckloff, B. W., Petersen, G. M. et al. (2013), ‘Genetic alterations associated with progression from pancreatic intraepithelial neoplasia to invasive pancreatic tumor’, *Gastroenterology* **145**(5), 1098–1109. [32](#)
- Newton, M. A., Noueir, A., Sarkar, D. & Ahlquist, P. (2004), ‘Detecting differential gene expression with a semiparametric hierarchical mixture method’, *Biostatistics* **5**(2), 155–176. [22](#)
- Park, Y., Figueroa, M. E., Rozek, L. S. & Sartor, M. A. (2014), ‘Methylsig: a whole genome dna methylation analysis pipeline’, *Bioinformatics* **30**(17), 2414–2422. [5](#)
- Perman, M., Pitman, J. & Yor, M. (1992), ‘Size-biased sampling of poisson point processes and excursions’, *Probability Theory and Related Fields* **92**(1), 21–39. [5](#), [9](#)
- Rackham, O. J., Dellaportas, P., Petretto, E. & Bottolo, L. (2015), ‘Wgbssuite: simulating whole-genome bisulphite sequencing data and benchmarking differential dna methylation analysis tools’, *Bioinformatics* **31**(14), 2371–2373. [23](#), [24](#)

- Rodriguez, A., B., D. D. & Gelfand, A. E. (2008), ‘The nested dirichlet process (with discussion)’, *Journal of the American Statistical Association* **103**, 1131–1144. [35](#)
- Saito, Y., Tsuji, J. & Mituyama, T. (2014), ‘Bisulfighter: accurate detection of methylated cytosines and differentially methylated regions’, *Nucleic Acids Research* p. gkt1373. [5](#)
- Sethuraman, J. (1994), ‘A constructive definition of dirichlet priors’, *Statistica Sinica* pp. 639–650. [12](#)
- Siegel, R. L., Miller, K. D. & Jemal, A. (2017), ‘Cancer statistics, 2017’, *CA: A Cancer Journal for Clinicians* **67**(1), 7–30. [3](#)
- Song, Q., Decato, B., Hong, E. E., Zhou, M., Fang, F., Qu, J., Garvin, T., Kessler, M., Zhou, J. & Smith, A. D. (2013), ‘A reference methylome database and analysis pipeline to facilitate integrative and comparative epigenomics’, *PloS One* **8**(12), e81148. [5](#)
- Subramaniam, S. & Hsiao, G. (2012), ‘Gene-expression measurement: variance-modeling considerations for robust data analysis’, *Nature Immunology* **13**(3), 199–203. [33](#)
- Sun, D., Xi, Y., Rodriguez, B., Park, H. J., Tong, P., Meong, M., Goodell, M. A. & Li, W. (2014), ‘Moabs: model based analysis of bisulfite sequencing data’, *Genome Biology* **15**(2), R38. [5](#)
- Tao, K., Wu, C., Wu, K., Li, W., Han, G., Shuai, X. & Wang, G. (2012), ‘Quantitative analysis of promoter methylation of the ednrb gene in gastric cancer’, *Medical Oncology* **29**(1), 107–112. [32](#)
- Teh, Y. W., Jordan, M. I., Beal, M. J. & Blei, D. M. (2006), ‘Hierarchical dirichlet processes’, *Journal of the American Statistical Association* **101**, 1566–1581. [9](#), [35](#), [43](#)
- Tomlinson, G. & Escobar, M. (2003), ‘Analysis of densities’, *Talk given at the Joint Statistical Meeting* **103**, 1131–1144. [35](#)

- Tsunoda, S., Smith, E., De Young, N. J., Wang, X., Tian, Z.-Q., Liu, J.-F., Jamieson, G. G. & Drew, P. A. (2009), ‘Methylation of *cldn6*, *fbn2*, *rbp1*, *rbp4*, *tfpi2*, and *tmeff2* in esophageal squamous cell carcinoma’, *Oncology Reports* **21**(4), 1067–1073. [32](#)
- Vedeld, H. M., Goel, A. & Lind, G. E. (2017), Epigenetic biomarkers in gastrointestinal cancers: The current state and clinical perspectives, *in* ‘Seminars in cancer biology’, Elsevier. [3](#)
- Vrana, D., Hlavac, V., Brynychova, V., Vaclavikova, R., Neoral, C., Vrba, J., Aujesky, R., Matzenauer, M., Melichar, B. & Soucek, P. (2018), ‘Abc transporters and their role in the neoadjuvant treatment of esophageal cancer’, *International Journal of Molecular Sciences* **19**(3), 868. [32](#)
- Wang, D., Yan, L., Hu, Q., Sucheston, L. E., Higgins, M. J., Ambrosone, C. B., Johnson, C. S., Smiraglia, D. J. & Liu, S. (2012), ‘Ima: an r package for high-throughput analysis of illumina’s 450k infinium methylation data’, *Bioinformatics* **28**(5), 729–730. [4](#)
- Warden, C. D., Lee, H., Tompkins, J. D., Li, X., Wang, C., Riggs, A. D., Yu, H., Jove, R. & Yuan, Y.-C. (2013), ‘Cohcap: an integrative genomic pipeline for single-nucleotide resolution dna methylation analysis’, *Nucleic Acids Research* **41**(11), e117–e117. [4](#), [27](#)
- Yu, X. & Sun, S. (2016), ‘Hm-dm: identifying differentially methylated regions using a hidden markov model’, *Statistical Applications in Genetics and Molecular Biology* **15**(1), 69–81. [5](#)
- Zeger, S. L. & Karim, M. R. (1991), ‘Generalized linear models with random effects: A gibbs sampling approach’, *Journal of the American Statistical Association* **86**, 79–86. [34](#)